

Displaced clines in an avian hybrid zone (Thamnophilidae: *Rhegmatorhina*) within an Amazonian interfluve

Glaucia Del-Rio,^{1,2,3}  Marco A. Rego,^{1,2}  Bret M. Whitney,^{1,4}  Fabio Schunck,⁴  Luís F. Silveira,⁴ 
Brant C. Faircloth,^{1,2}  and Robb T. Brumfield^{1,2} 

¹Museum of Natural Science, Louisiana State University, Baton Rouge, Louisiana 70803

²Department of Biological Sciences, Louisiana State University, Baton Rouge, Louisiana 70803

³E-mail: glaucia.ornito@gmail.com

⁴Museu de Zoologia, Universidade de São Paulo, São Paulo, SP 04263-000, Brazil

Received December 20, 2020

Accepted September 1, 2021

Secondary contact between species often results in the formation of a hybrid zone, with the eventual fates of the hybridizing species dependent on evolutionary and ecological forces. We examine this process in the Amazon Basin by conducting the first genomic and phenotypic characterization of the hybrid zone formed after secondary contact between two obligate army-ant-followers: the White-breasted Antbird (*Rhegmatorhina hoffmannsi*) and the Harlequin Antbird (*Rhegmatorhina berlepschi*). We found a major geographic displacement (~120 km) between the mitochondrial and nuclear clines, and we explore potential hypotheses for the displacement, including sampling error, genetic drift, and asymmetric cytonuclear incompatibilities. We cannot exclude roles for sampling error and genetic drift in contributing to the discordance; however, the data suggest expansion and unidirectional introgression of *hoffmannsi* into the distribution of *berlepschi*.

KEY WORDS: Antbirds, asymmetric introgression, introgressive hybridization, moving hybrid zone.

Hybrid zones are geographically limited regions of introgressive hybridization found at the interface of two or more biological distributions. They are aptly characterized as natural laboratories of speciation (Hewitt 1988) because they provide an opportunity to study, in wild populations of organisms, the evolutionary and ecological dynamics associated with hybridization after secondary contact. Inferences about the evolutionary forces that generate and maintain the structure of a hybrid zone can be made by characterizing and analyzing genomic and phenotypic patterns from a set of samples spanning the zone (Szymura and Barton 1986). These same analyses allow inferences concerning the ultimate fate of the hybrid zone, which includes reticulation of the two taxa into a single taxon, genetic swamping of one taxon by the other, or formation of an equilibrium hybrid zone.

Most hybrid zone analyses are conducted within the conceptual framework of cline theory. After secondary contact with hybridization occurs between differentiated taxa, clinal charac-

ter transitions develop across the hybrid zone as their genomes and phenotypes recombine. If there is no selection against hybrids, the initially steep clines in the zone should decay at a rate proportional to the dispersal rate (Endler 1977; Barton and Gale 1993), eventually vanishing into a reticulate species (Endler 1977). Alternatively, if there are asymmetries in population densities, dispersal ability, or competition, genetic swamping of one of the hybridizing species will occur. Clines from loci throughout the genome are not expected to have similar cline widths and centers, because recombination breaks up linked parental allele combinations.

If there is selection against hybrids, the conceptual theory associated with the widely adopted (McEntee et al. 2020) tension zone hybrid zone model (Barton and Gale 1993) can be used to make inferences about the forces structuring the zone. A central component of the tension zone model is that a stable hybrid zone is possible through the opposing forces of reduced hybrid

fitness, which narrows the zone, and the influx of parentals, which widens the zone. All genetic clines in tension zones are expected to have similar geographic centers and widths. This expectation is based on an assumption of coupling (Butlin and Smadja 2018) in which barrier loci occur throughout the genome and the physical and epistatic linkages among them extend their effects to the entire genome. As the number and genomic distribution of barrier loci decreases, the effect of coupling also decreases, and one would expect greater variance in the centers and widths of character clines.

Geographically, tension zones, even at equilibrium, are expected to move due to stochastic forces such as genetic drift. The geographic landscape is not an explicit part of the model. However, tension zones, regardless of whether they are at equilibrium, are expected to move to a point where the number of parentals dispersing into the zone is equivalent between the species. This often occurs at an ecotone or environmental bottleneck where the densities of the two species are similar. In the tension zone literature, this area is often referred to as a population density trough. Tension zones would also be expected to move if the hybridization is due to a biological invasion, in which case the zone moves toward the invader as its genome becomes asymmetrically integrated into the invader (Currat et al. 2008). Beyond dispersal dynamics, other asymmetries, such as in hybrid fitness, can also lead to hybrid zone movements, including displacement of cytoplasmic and nuclear cline centers from one another (Toews and Brelsford 2012).

Direct tests of hybrid fitness in avian hybrid zones have only been achieved in a handful of logistically challenging studies (Bronson et al. 2005). Thus, most inferences about hybrid fitness are made indirectly, such as by the presence of displaced clines or particular genotypes in the hybrid zone. For example, a preponderance of F1 individuals at the hybrid zone center suggests hybrids are sterile or that backcrosses suffer from reduced hybrid fitness (Pulido-Santacruz et al. 2018; Cronemberger et al. 2020); otherwise the center is expected to be a hybrid swarm composed entirely of advanced generation hybrids and backcrosses (Harrison 1993).

Here, we present the first genetic and phenotypic characterization of a hybrid zone between two obligate army-ant-followers in southern Amazonia: the White-breasted Antbird (*Rhegmatorhina hoffmannsi*) and the Harlequin Antbird (*Rhegmatorhina berlepschi*). The two species are easily distinguishable by their chest and throat colors: *hoffmannsi* has a white chest and throat, whereas *berlepschi* has a rufous brown chest and a black throat. Their entire distributions occur within the interfluvium of the Madeira and Tapajós Rivers, two of the Amazon river's major tributaries (Fig. 1). *Rhegmatorhina berlepschi* is found from the west bank of the middle and lower Tapajós River, west to the east bank of the Sucunduri River, then south to near the Sucun-

duri headwaters. *Rhegmatorhina hoffmannsi* occupies the region between the east bank of the Madeira River and the west bank of the Sucunduri River, then south to well beyond the headwaters of the Sucunduri and extending eastward to an unknown extent east of the middle Juruena River. Until field observations by BMW in 2004 revealed the presence of birds with intermediate plumage near the Sucunduri River, it was unclear whether the two species came into secondary contact.

Our primary goals were to characterize the genotypic and phenotypic structure of the *Rhegmatorhina* hybrid zone by conducting geographic and genomic cline analyses, demographic modeling, and analyses of the genomic composition of individuals in the zone. We also assess the possibility of displaced mitochondrial and nuclear clines suggested by patterns of mitochondrial haplotypes (Ribas et al. 2018). Although they did not collect samples from the hybrid zone, Ribas et al. (2018) found a deep mitochondrial break within parental populations of *hoffmannsi* approximately 150 km south of where BMW observed birds with intermediate plumage—observations that could indicate discordant mitochondrial and phenotypic clines. We examine whether genetic variation in the hybrid zone is best explained by neutral diffusion, by a nonequilibrium tension zone, or by a tension zone at equilibrium.

Materials and Methods

SAMPLING

From 2005 to 2018, GDR, MAR, BMW, FS, and LFS collected 162 specimens spanning the transition from parental *hoffmannsi* to parental *berlepschi*. Voucher specimens were archived at the Louisiana State University Museum of Natural Science and the Museu de Zoologia da Universidade de São Paulo (Table S1). For each specimen, we prepared a round skin and preserved pectoral muscle, heart, and liver tissues in liquid nitrogen and 95% ethanol. To supplement our sampling, we received loans of 35 tissue samples from the Museu Paraense Emílio Goeldi (Belém, Brazil), 21 tissue samples from the Instituto Nacional de Pesquisa da Amazônia (Manaus, Brazil), and five tissue samples from the Field Museum of Natural History (Chicago, IL), bringing our total sample to 222 vouchered individuals collected from 86 localities (Table S1). We included tissue samples from three outgroups: *Rhegmatorhina melanosticta* (three individuals), *Rhegmatorhina gymnops* (three individuals), and *Rhegmatorhina cristata* (one individual; Table S1).

DEFINING A TRANSECT OF POPULATION SAMPLES ACROSS THE HYBRID ZONE

We defined 22 population samples from the 86 collection localities by constructing a 35 km buffer around each specimen

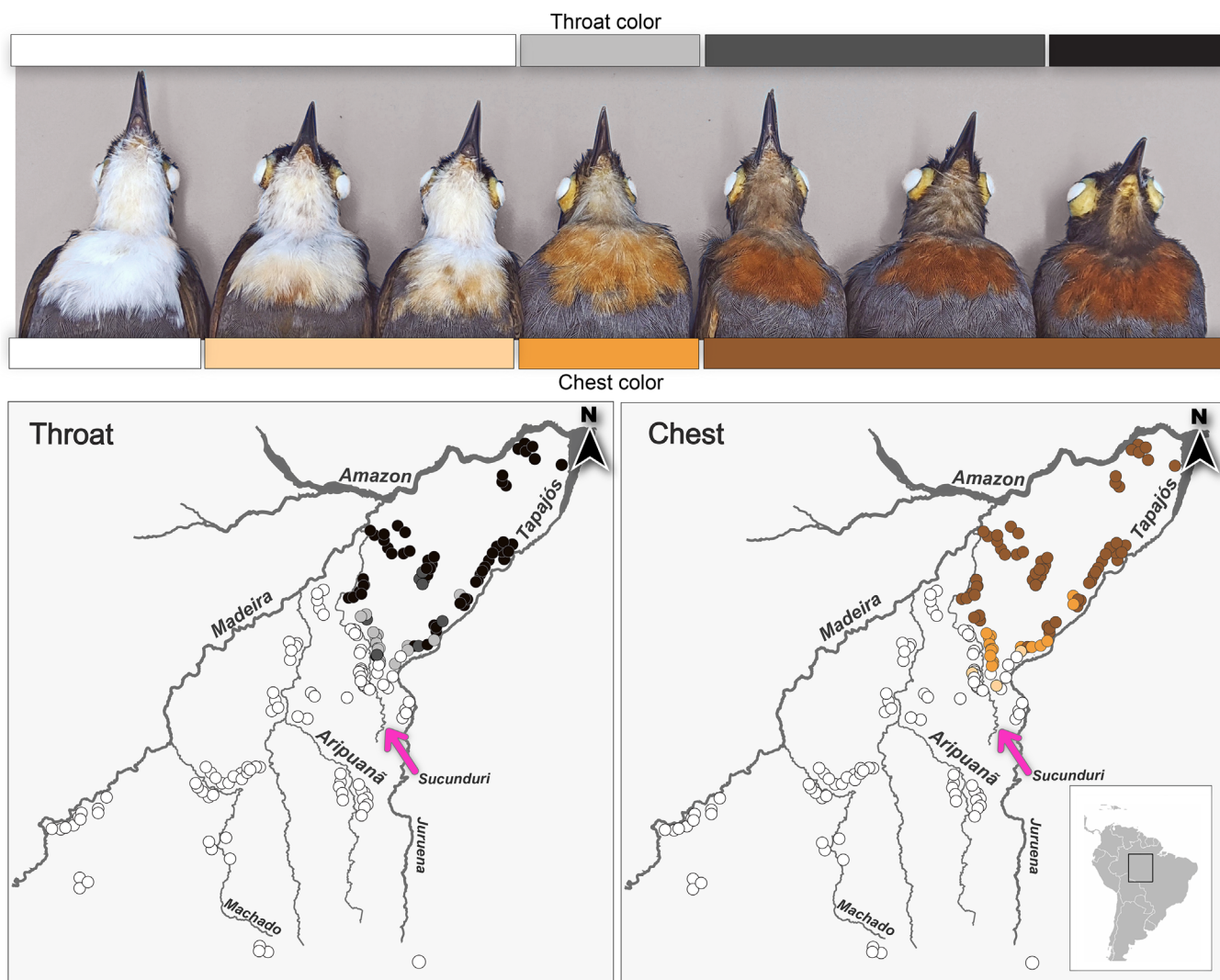


Figure 1. Plumage variation in the *Rhegmatorhina* hybrid zone. Top panel shows the range of throat and chest color variation across the hybrid zone. Circles indicate individual collection localities, and fill color illustrates where variants are found geographically. Pink arrow indicates the Sucunduri River headwaters.

locality using buffer analysis in ArcGIS 10.6 (Fig. S1A, B). Where buffers overlapped on the same side of each river bank, we grouped specimens in the joint buffer area into a single population, and we defined the “center” of the population as the geometric center of the joint buffer area.

Because we were interested in characterizing clinal transitions in genotypes and phenotypes across the hybrid zone, we needed to define a linear transect that extended from population samples of parental *hoffmannsi* to population samples of parental *berlepschi*. To construct the transect, we drew a straight line connecting *hoffmannsi* in the south to *berlepschi* in the north. To define the angle at which the transect would be positioned across the interfluvium, we used kriging in ArcGIS 10.6 to interpolate estimates of the ancestry coefficient across the landscape, plotted the 0.5 kriging isocline, and drew lines connecting the isocline to all

sampling localities (Fig. S1C). Then, we calculated the average slope of lines connecting the median isocline to sampling localities with ArcGIS 10.6, and we used the average slope as the angle of the transect across the hybrid zone. We then determined the location of each population sample along the transect by drawing a perpendicular line from the transect to the geographic center of each of the 22 population samples described above. Because this procedure would place locality 7, which is on the left bank of the Aripuanã River, after localities 10 and 12, which are on the right bank of the Aripuanã, we merged localities 7 and 8 into a single “left bank” population sample. The logic behind this decision is that the order in which transect localities are positioned along the transect should be prioritized by left-to-right-bank orientation—specifically that all localities on the left bank of a river should precede any locality on the right bank of the same river. After

merging localities 7 and 8, we obtained a final number of 21 populations along the transect (Fig. S1D; Table 1). To facilitate cline comparisons among traits, we “zeroed” the geographic distance axis for the transect at the point where the mitochondrial transition occurs (i.e., at the Aripuanã River), with samples north of the river having positive values and samples south of the river having negative values.

COLLECTION OF PLUMAGE COLOR AND MORPHOMETRIC DATA

To characterize the phenotypic structure of the hybrid zone, we collected mensural and colorimetric data from 184 of the 222 specimens after excluding 23 specimens in juvenile plumage and 15 specimens whose condition did not allow accurate measurements (Table S1). We measured eight morphometric characters using a dial caliper (0.1 mm precision): tail length, wing length, tarsus length, culmen length, distance from nare to tip, and bill base width. We tested for significant differences in these characters between sexes and between parental populations of the two species (i.e., we compared population 1 to population 21) by visual inspection of boxplots for each group and an analysis of variance with Tukey’s Honestly Significant Difference (HSD) test to compare pairwise mean of each factor (R Core Team 2019).

To collect data on color reflectance, we calibrated an Ultrascan sphere reflectance spectrophotometer (Hunter Labs, Inc., Reston, VA) using a pure white reflecting surface (Ocean Optics white standard) and measured color reflectance from 300 to 700 nm in each of eight plumage patches: crown, mantle, rectrices, belly, chest, throat, wing coverts, and primaries. For each patch, we summarized percentage reflectance by averaging three independent measurements using pavo 2.0 (Maia et al. 2019). We compared average plumage reflectance in males and females by visual inspection of boxplots and an analysis of variance with Tukey’s HSD test (R Core Team 2019).

COLLECTION AND ANALYSIS OF MITOCHONDRIAL DATA

To characterize mitochondrial DNA structure across the hybrid zone, we extracted DNA from 195 individuals of *Rhegmatorhina* and six outgroup samples (Table S1) using Qiagen DNeasy Blood & Tissue extraction kits (Qiagen, Valencia, CA) following the manufacturer’s protocol. After extraction, we amplified 1041 base pairs (bp) of the mitochondrial gene NADH dehydrogenase subunit 2 (ND2) using primers L05215 and HTrpC (5’-CGGACTTTAGCAGAACTAAGAG-3’) or H06313 (Sorenson et al. 1999) in a 25 μ L PCR reaction with 2.5 μ L of template DNA (~50 ng), 1 μ L of each primer (10 mM), 1 μ L of 2.5 mM (each) dNTPs, 2.5 μ L of reaction buffer with MgCl₂ (15 mM), and 0.1 U of NEB HotStart Taq DNA polymerase (5 U/ μ L). We used a thermocycling profile of 94°C for 5 min, followed by 34

cycles of 94°C for 30 s, 60 s of annealing at 54°C, 60 s at 72°C, and a 10-min final extension at 72°C. We then had a commercial facility (Macrogen Corp.) purify PCR products with Exo-SAP (Thermo Fisher Scientific, Inc.) and Sanger sequence (forward and reverse) purified products using capillary electrophoresis on an Applied Biosystems 3730xl Genetic Analyzer (Thermo Fisher Scientific, Inc.).

We used Geneious R10 (<https://www.geneious.com>) to align forward and reverse sequences to a reference *R. hoffmannsi* ND2 sequence (GenBank MG603845). We excluded base calls with PHRED scores below 30, and we removed sequences of eight individuals (Table S1) because they were shorter than the total length of ND2. We used MUSCLE (Edgar 2004) to generate a consensus sequence from forward and reverse sequences of each individual, aligned consensus sequences among individuals using Geneious Alignment (2020.1.1), and reconstructed an ND2 phylogenetic tree using BEAST 2 (Bouckaert et al. 2014) with the GTR + γ finite-sites substitution model, 100 million iterations, and sampling from the posterior distribution every 1,000 iterations. We removed the first 10% of posterior samples as burn-in; we checked convergence of the remaining posterior sample with Tracer (Rambaut et al. 2014), considering that the run converged when ESS values were ≥ 200 (Drummond et al. 2006); and we estimated a maximum clade credibility tree with TreeAnnotator (2.5.1). To visualize the relationships between mitochondrial haplotypes and the number of mutations separating them, we constructed a haplotype network using the program PopART (Leigh and Bryant 2015) with the TCS algorithm (Clement et al. 2002).

RADseq LIBRARY PREPARATION AND SEQUENCING

To investigate nuclear genetic structure and allele frequencies for the largest possible sample of individuals across the hybrid zone, we collected RADseq (Baird et al. 2008) data from the 222 *Rhegmatorhina* individuals described in the “Sampling” section. Before preparing RADseq libraries, we evaluated the quality of DNA extracts by visualizing each on 1.5% agarose gels, and we considered samples having fragment lengths >1.5 kbp adequate for library preparation. We excluded extracts from 10 samples that fell below this size range (Table S1), and we constructed 3RAD (Bayona-Vásquez et al. 2019) libraries for the remaining 212 samples using *Xba*I and *Eco*RI-HF, with *Nhe*I to reduce formation of adapter dimers. We cleaned ligation products using Sera-Mag Speed-Beads (Rohland and Reich 2012) at a ratio of 1.25:1 (v/v), and we created full-length libraries by amplifying the ligation products with 11 PCR cycles using iTru5 and iTru7 as described in Glenn et al. (2017). We quantified PCR-amplified libraries using a Qubit Fluorometer (Life Technologies, Inc.) and checked for valid constructs by visualizing each library on 1.5% agarose gels to ensure fragment distributions spanned 300–800 bp. After validation, we cleaned amplified libraries using

Table 1. Data used for geographic cline analysis. Average percent chest and throat reflectance (600 nm), average ancestry coefficient (SNMF results), allele frequencies for the *berlepschi* mtDNA haplotype, and allele frequencies for the top five diagnostic loci for each transect locality. Average ancestry coefficient is based on 8,773 SNPs. Sample size within parentheses. Sample size for ancestry coefficient equal to sample size for calculation of allele frequencies in each population.

Population	Transect distance (km)	Chest reflectance	Throat reflectance	Ancestry coefficient	mtDNA	SNP1	SNP2	SNP3	SNP4	SNP5
West of Aripuanã River	1	55 ± 4 (N = 4)	36 ± 3 (N = 4)	0.001 ± 0.00 (N = 8)	0.00	0.00	0.06	0.00	0.00	0.00
	2	49 ± 5 (N = 5)	37 ± 4 (N = 5)	0.001 ± 0.02 (N = 8)	0.00	0.00	0.00	0.00	0.00	0.00
	3	45 ± 7 (N = 2)	31 ± 10 (N = 2)	0.073 ± 0.03 (N = 3)	0.00	0.00	0.00	0.00	0.17	0.00
	4	44 ± 2 (N = 6)	34 ± 5 (N = 6)	0.004 ± 0.01 (N = 7)	0.00	0.00	0.14	0.00	0.00	0.00
	5	49 ± 4 (N = 5)	27 ± 4 (N = 5)	0.002 ± 0.05 (N = 5)	0.00	0.00	0.40	0.00	0.00	0.00
	6	53 ± 2 (N = 5)	37 ± 3 (N = 5)	0.090 ± 0.02 (N = 5)	0.00	0.00	0.25	0.00	0.13	0.00
	7	39 ± 0 (N = 1)	31 ± 0 (N = 1)	0.129 ± 0.00 (N = 1)	0.00	0.50	0.00	0.00	0.00	0.00
	8	48 ± 4 (N = 8)	33 ± 7 (N = 8)	0.067 ± 0.03 (N = 10)	0.00	0.00	0.00	0.05	0.00	0.00
	9	53 ± 4 (N = 4)	33 ± 7 (N = 4)	0.132 ± 0.02 (N = 5)	0.00	0.00	0.20	0.00	0.00	0.00
Between Aripuanã and Sucunduri	10	51 ± 6 (N = 10)	33 ± 8 (N = 10)	0.268 ± 0.03 (N = 11)	0.63	0.55	0.41	0.23	0.23	0.23
	11	49 ± 5 (N = 5)	29 ± 2 (N = 5)	0.469 ± 0.02 (N = 5)	1.00	0.50	0.30	0.40	0.10	0.38
	12	45 ± 12 (N = 14)	29 ± 11 (N = 14)	0.531 ± 0.02 (N = 15)	1.00	0.50	0.43	0.40	0.20	0.04
	13	52 ± 4 (N = 4)	34 ± 6 (N = 4)	0.564 ± 0.03 (N = 5)	1.00	0.80	0.40	0.80	0.10	0.38
	14	51 ± 4 (N = 2)	35 ± 4 (N = 2)	0.480 ± 0.01 (N = 3)	1.00	1.00	0.17	1.00	0.00	0.17
	15	10 ± 5 (N = 5)	3 ± 1 (N = 5)	0.876 ± 0.04 (N = 7)	1.00	0.79	0.64	0.79	0.57	0.79
East bank of Sucunduri River	16	20 ± 11 (N = 19)	16 ± 12 (N = 19)	0.698 ± 0.08 (N = 21)	1.00	0.71	0.57	0.55	0.52	0.43
	17	20 ± 10 (N = 11)	11 ± 8 (N = 11)	0.790 ± 0.08 (N = 11)	1.00	0.82	0.82	0.77	0.55	0.59
	18	11 ± 2 (N = 10)	2 ± 0 (N = 10)	0.934 ± 0.04 (N = 10)	1.00	1.00	0.60	0.75	1.00	1.00
	19	12 ± 2 (N = 21)	3 ± 1 (N = 21)	0.901 ± 0.03 (N = 23)	1.00	0.96	0.80	0.89	0.83	1.00
	20	10 ± 2 (N = 9)	2 ± 0 (N = 9)	0.964 ± 0.03 (N = 9)	1.00	0.94	0.83	0.61	0.83	0.94
	21	12 ± 2 (N = 5)	1 ± 1 (N = 5)	0.990 ± 0.01 (N = 8)	1.00	1.00	1.00	0.94	1.00	1.00

Speed-Beads at a 1:1 ratio (v/v) and pooled all libraries. To reduce the total number of RADseq loci recovered, we had a commercial service (Georgia Genomics Facility, Athens, GA) divide the pool of libraries across four lanes of a Pippin Prep (Sage Science, Beverly, MA) and perform size selection using a 1.5% dye-free Marker K agarose gel cassette (CDF1510) set to capture fragments $550 \text{ bp} \pm 10\%$. After size selection, GGF staff combined all lanes of size-selected products and increased the concentration of size-selected libraries by performing six cycles of PCR recovery using standard Illumina P5 and P7 primers. GGF staff cleaned the resulting reaction product, quantified the size-selected pool using a commercial library quantification kit (F. Hoffmann-La Roche AG, Basel, Switzerland), and prepared a $10 \mu\text{M}$ pool of libraries for paired-end (PE) 150 bp sequencing across two lanes of Illumina HiSeq 3000 sequencing at the Oklahoma Medical Research Foundation (Oklahoma City, OK).

WHOLE GENOME SEQUENCING

Because RADseq data can be difficult to analyze de novo (Shafer et al. 2017), we sequenced a reference *R. hoffmannsi* genome to facilitate RADseq analyses and also to serve as an exemplar for family Thamnophilidae as part of ongoing B10K analyses (Feng et al. 2020). Briefly, we sent a flash-frozen liver sample of a female *hoffmannsi* (LSUMNS 192276) to Dovetail Genomics, LLC where they extracted high-molecular weight DNA to prepare one short-insert library for Illumina sequencing along with one proprietary “Chicago” library for scaffolding. They sequenced both libraries using the Illumina HiSeq X platform (PE 150) and performed an initial assembly (NCBI GCA_013398505.1) using Meraculous (version 2.2.5) and their proprietary HiRise scaffolding software (October 2017 version). Preliminary analyses of our RADseq data suggested that the Dovetail assembly contained few fragments of the Z chromosome, potentially due to the Dovetail Meraculous contig assembly pipeline. We verified this observation of missing Z contigs by aligning the Dovetail assembly to the *Chiroxiphia lanceolata* assembly (NCBI PRJNA561943, NCBI GCA_009829145.1) from the Vertebrate Genomes Project (VGP) (Rhie et al. 2021) using RaGOO 1.1 (Alonge et al. 2019), and the results of this analysis showed that the Dovetail contigs only aligned to 1.2% (868 kbp) of the *Chiroxiphia* Z chromosome. As a result, we re-assembled the Dovetail data using a different contig assembly approach to recover a larger fraction of the Z chromosome. Specifically, we trimmed the short-insert and Chicago sequence data (NCBI SRX6608225, SRX88182620) to remove adapters and low-quality bases using Trimmomatic (Bolger et al. 2014). After trimming, we corrected the short insert reads with Musket 1.1 and a kmer value of 61 (Liu et al. 2013) because we had difficulty getting the Spades 3.14.0 (Nurk et al. 2013) error-correction algorithm to process all of the trimmed, short-insert sequence data. After correction, we assembled the corrected, short-

insert reads with Spades 3.14.0 (Nurk et al. 2013) and scaffolded Spades contigs longer than 1,000 bp using BESST 2.2.8 (Sahlin et al. 2014) because preliminary tests suggested BESST outperformed the Spades scaffolding algorithm. We performed a second round of scaffolding with the Dovetail “Chicago” data and Salsa 2.2 (Ghurye et al. 2017). After the second round of scaffolding, we polished the assembly with Pilon 1.23 using the trimmed, short-insert data; we identified and modeled transposable element families with RepeatModeler 2.0.1 (<http://www.repeatmasker.org/RepeatModeler/>); and we soft-masked repeats using these models, RepeatMasker open-4.0.9 (<http://www.repeatmasker.org>), and NCBI/RMBLAST 2.9.0+ (Altschul et al. 1990). Finally, we used RaGOO to build chromosomal pseudomolecules from the masked scaffolds using the VGP assembly of *Chiroxiphia lanceolata* (NCBI GCA_009829145.1) as a reference, and we compared these results to the earlier pseudo-chromosomal scaffolds we built from the Dovetail contigs to determine if we assembled a more complete Z chromosome. We evaluated statistics for our new assembly with Quast 5.0.2, and we used BUSCO 4.0.6 (eukaryota_odb10) to estimate assembly completeness for both our new assembly and the initial Dovetail assembly.

VARIANT CALLING AND FILTERING

To call variants in the RADseq data, we used programs in the software package STACKS 1.48 (Catchen et al. 2013). Specifically, we used “*process_radtags*” to demultiplex our 3RAD data, clean sequences, and trim low-quality bases. We then aligned clean reads (i.e., reads 1 and 2 for each individual) to our pseudo-chromosomal *R. hoffmannsi* reference assembly using BWA-MEM 0.7.17 (Li 2013) and default parameters for all arguments. We filtered alignments with samtools 1.10 by keeping only uniquely mapping reads and removing reads that were soft-clipped, had map qualities below 25, were unmapped, or contained ≥ 5 SNPs per read. After alignment filtering, we used “*pstacks*” to extract RAD stacks that were successfully aligned to the reference genome (minimum depth of coverage = 3) and to detect SNPs. We created a catalog of consensus loci with “*cstacks*” (number of mismatches allowed between sampled loci = 1), and we matched all samples in the population against the catalog using “*sstacks*.” We then used the “*populations*” program to export SNP data for all 212 individuals in variant call format (VCF), where we set the minimum minor allele frequency (MAF) to process a nucleotide site to 0.02. STACKS parameters not mentioned above were left at default values.

We used VCFtools 0.1.13 (Danecek et al. 2011) to remove indels from the resulting VCF file. Because missing data, low coverage, and minimum allele count strongly affect genetic structure inference (Chattopadhyay et al. 2014; Linck and Battey 2019), we also used VCFtools to remove loci that were missing data for more than 10% of the individuals (*-max-missing*

= 0.90), had coverage below $15 \times (-minDP = 15)$, and had a minor allele count less than 3 ($-mac = 3$) (Linck and Battey 2019).

Because linkage disequilibria (LD) can affect the accuracy of ancestry estimates in admixture methods (Frichot et al. 2014), we used the “*indep-pairwise*” function in plink 2.0 (Chang et al. 2015) to produce a subset of loci in approximate linkage equilibrium by setting the window size to 50 variants, the variant count to shift the window at the end of each step to 5, and the pairwise R^2 threshold to 0.5 (modified from Wang et al. 2020). Then, we used VCFtools to filter the list of all SNPs to this subset. We also used VCFtools to remove SNPs deviating from Hardy-Weinberg Equilibrium (HWE, $P < 0.05$) based on a test of heterozygote excess (*-hardy*) (Wigginton et al. 2005), because departures from HWE can indicate genotyping error (Chen et al. 2017). Finally, we used VCFtools to exclude 32 individuals from our dataset that were missing more than 5% of the total number of SNPs obtained after all filtering steps (Table S1). We performed all analyses, except demographic inferences, with this set of variant sites. Because VCF files filtered for minor allele count will produce a truncated site frequency spectrum (SFS), we created a second SNP dataset that we input to momi2 (described below) using all filtering steps, except for the minor allele count filter.

SUMMARY STATISTICS AND ANALYSES OF GENETIC VARIATION

We computed average allele frequencies for each population sample along the geographic transect using “*makefreq*” in adegenet 2.1.2 (Jombart and Ahmed 2011). We used these allele frequencies to identify a set of filtered, “diagnostic” SNP loci, which we defined as the set of SNP loci having an average allele frequency < 0.2 at locality 1 (the southernmost *hoffmannsi* population) and > 0.8 at localities 20 and 21 (the northernmost *berlepsi* populations). We defined a more stringent set of diagnostic SNP loci having an average allele frequency < 0.1 at locality 1 and > 0.9 at localities 20 and 21. We separated diagnostic SNPs into autosomal and Z-linked groups based on their pseudo-chromosomal position, and we used the program HWadmiX (Backenroth and Carmi 2019) to test for Hardy-Weinberg proportions for each population sample at each stringent, Z-linked diagnostic SNP. To conduct the same test for autosomal SNPs, we used VCFtools function *-hardy* (Wigginton et al. 2005). A deficiency of heterozygotes is sometimes observed at the center of hybrid zones if hybrids have reduced fitness.

INFERRING POPULATION STRUCTURE FROM RADseq DATA

We input the filtered SNPs to sNMF (Frichot et al. 2014), which uses sparse nonnegative matrix factorization and least-squares optimization to calculate ancestry coefficients for each individual, calculate the number of genetic clusters that best fit the data

(k), and assign individuals to k ancestral populations (Frichot et al. 2014). We created pie-charts using ArcGis 10.6 to map the ancestry coefficients for each individual to their collection locality. We inferred the optimal number of ancestral populations for transect samples by testing a range of k values (1–5) with different α regularization parameters (10–10,000, in increments of 100). We selected this range of values because $k = 1$ represented a scenario of no genetic structure and $k = 5$ represented a scenario in which populations were structured by large rivers (Machado, Aripuanã, Sucunduri, Abacaxis). We performed 100 replicate runs for each $k + \alpha$ combination, and we determined the optimal k -value by plotting k against cross-entropy for different values of α and identifying the point where cross-entropy stopped decreasing. We also used discriminant analysis of principal components (DAPC) to estimate k using the “*find.clusters*” function in adegenet 2.0 (Jombart and Ahmed 2011). Specifically, we ran the k-means algorithm with increasing values of k (1–5) and selected the optimal value of k by minimizing the Bayesian Information Criterion (BIC) (Jombart and Ahmed 2011).

To classify individuals as F1s, backcrosses, or advanced-generation hybrids, we created triangle plots using the package Introgress (Gompert and Buerkle 2010, 2016). For each individual’s hybrid index, we used the ancestry coefficient, and we calculated interspecific heterozygosity for the stringent diagnostic loci using the function *-hardy* in VCFtools (Wigginton et al. 2005).

FITTING GEOGRAPHIC CLINES TO THE MORPHOLOGICAL AND MOLECULAR DATA

We used HZAR (Derryberry et al. 2014) to fit equilibrium cline models (Szymura and Barton 1986; Barton and Gale 1993; Gay et al. 2008) to mitochondrial haplogroup frequency, allele frequencies at diagnostic nuclear SNPs, the mean ancestry coefficient, and mean chest and throat color (Table 1). We ran the MCMC model-fitting procedure in HZAR using default settings for chain length (1×10^6), burn-in (1×10^4), and thinning (100), and we selected the model that best fit the data using the Akaike Information Criterion corrected for small sample size (AICc) (Burnham and Anderson 2002). For the haplotype and allele frequency data, we evaluated 16 different models, and for chest/throat color and ancestry coefficient, six different models (Table S2). We used the best fit (lowest AICc) model to estimate cline centers and cline widths along with 95% confidence intervals (Szymura and Barton 1986). We determined statistical differences in cline centers by visual observation of nonoverlapping 95% confidence intervals.

We also tested for statistically significant differences between the mitochondrial and nuclear cline centers by refitting the nuclear clines (estimated above) with the cline center fixed to the confidence interval of the mitochondrial cline (HZAR

function “*hzar.model.addCenterRange*”) (Derryberry et al. 2014). We used a likelihood ratio test in R with one degree of freedom to determine whether the fit of “fixed” cline centers was different from the “unfixed” cline centers for each nuclear locus. We also tested for cline center discordance across traits using the composite likelihood method described by Phillips et al. (2004). With the HZAR function “*hzar.profile.dataGroup*,” we constructed log-likelihood profiles for each trait (plumage color, mtDNA, ancestry coefficient, diagnostic loci), fixing cline centers at each 20 km along the transect. We summed log-likelihoods across traits to construct a composite log-likelihood profile. We then compared the maximum likelihood (ML) value of the composite log-likelihood profiles (*MLcomp*) with the sum of all MLEs (maximum likelihood estimate for the best cline model) for different traits (*MLsum*). If the clines of different traits have the same center, *MLcomp* should not be significantly different from *MLsum*. If the clines do not have the same center, *MLcomp* will be significantly smaller than *MLsum*. We determined the significance of differences between *MLcomp* and *MLsum* using a likelihood ratio test in R, with $n - 1$ degrees of freedom, where n is the sum of the number of SNPs plus one, which represents the mtDNA haplotype ($\alpha = 0.05$) (Kawakami et al. 2009).

To assess quality of cline fits among different traits (throat color, chest color, mtDNA, and the diagnostic SNPs), we made a bivariate plot with the confidence intervals for cline width on the X-axis and the confidence intervals for cline center on the Y-axis. We considered clines with the tightest confidence intervals for both center and width to be those with the best fit. This process also allowed us to detect outlier clines.

NEUTRAL DIFFUSION

Assuming a time of secondary contact, one can predict the expected width of geographic clines under a neutral model in which there are no reproductive isolating mechanisms. Clines narrower than expected under neutral expectations may be maintained by natural selection. The neutral diffusion model posits that in the absence of a barrier to gene flow, the width of a geographic cline increases in proportion to the root-mean-square natal dispersal distance of the organism (Barton and Gale 1993). The expected cline width for a fixed autosomal allele under the neutral diffusion model can be estimated using the equation:

$$w = 2.51\sigma\sqrt{t},$$

where w = width, σ is the standard deviation of the natal dispersal distance, and t is the number of generations since secondary contact (Barton and Gale 1993). We assumed a generation time of two years (Johnson and Wolfe 2018), and $\sigma = 2$ km based on population studies of the Chestnut-backed Antbird (*Poliocrania exsul*) (Woltmann et al. 2010). We explored a range of generations

since secondary contact (t): 20,000 years, equivalent to 10,000 generations; and 4,000 years, equivalent to 2,000 generations.

GENOMIC CLINE FITTING

While geographic clines capture the changes in allele frequencies across a transect, genomic clines measure the movement of ancestry blocks into different genomic backgrounds (Szymura and Barton 1986; Gompert et al. 2012) and can reveal patterns of introgression of loci from an “invader” species over the genomic background of an “invaded” species. To estimate genomic clines, we used the nuclear (i.e., autosomal and Z-linked) ancestry coefficient for each individual, calculated with sNMF, as the average genome-wide ancestry S . Then, we used the “logit-logistic” function to describe genomic clines for each locus i in terms of the average genome-wide ancestry S (Bazykin 1969):

$$\text{logit}(p_i) = v_i \text{logit}(S) - u_i$$

where p_i is the proportion of copies of locus i inherited from one of the target populations (here *berlepschi*), v_i indicates the slope of p_i , and u_i indicates the relative difference in cline position relative to the inflection point (Fitzpatrick 2013b). We quantified loci with positive and negative values of u_i , where negative values represented *berlepschi* alleles moving into the genomic background of *hoffmannsi* and positive values represented *hoffmannsi* alleles moving into the genomic background of *berlepschi*.

We used the Hlest (Fitzpatrick 2013a) multivariate outlier detection model to identify markers affected by selection. This method considers whether a model fitted to a given locus deviates from the null hypothesis ($p_i = S$) more than expected from drift alone. In Hlest, the joint distribution of parameter estimates of the Barton cline (i.e., the geographic cline in which center and width are transformed to α and β , respectively) (Barton 2008; Fitzpatrick 2013b) is assumed to follow a multivariate normal distribution, and under this assumption, the squared Mahalanobis distances (D^2) of each locus follows a chi-squared distribution (Johnson and Wichern 1998). When the distribution of D^2 differs from the null distribution more than expected by chance, the locus is considered an outlier because its variation cannot be explained by drift alone (Gompert and Buerkle 2011). We considered that a locus was a statistical outlier when D^2 deviated from the quantile-quantile plot (Johnson and Wichern 1998; Fitzpatrick 2012, 2013b).

DEMOGRAPHIC MODELS

Because we were interested in testing for asymmetric introgression outside the framework of geographic and genomic cline analyses, we wanted to compare several different models of demographic scenarios. Before running these models, we estimated ancestral divergence times (τ) and population sizes (θ) using

G-PhoCS 1.3 (Generalized Phylogenetic Coalescent Sampler) (Gronau et al. 2011). G-PhoCS is a Bayesian approach that uses Markov Chain Monte Carlo (MCMC) to sample model parameters and genealogies based on a set of sequence alignments from neutrally evolving loci sampled throughout the genome.

To run G-PhoCS, we considered birds from the area along the west bank of the Aripuanã (individuals from populations 8 and 9) as *hoffmannsi* and birds from the northernmost localities (individuals from populations 20 and 21) as *berlepschi* (Table S1), and to increase computational efficiency, we performed analyses using a randomly sampled subset of five individuals from each parental species (i.e., populations 8 and 9, and 20 and 21) (Table S1). For randomly sampled individuals, we used the “populations” program in STACKS with the option *-phylip-var-all* to create alignments of all RADseq loci in PHYLIP format. Then, we used custom Python (Python Software Foundation 2021) code to create two randomly sampled sets of sequence data (with 6,000 and 10,000 RADseq loci) from the original PHYLIP alignments. These reduced datasets allowed us to ensure computational tractability while also enabling us to assess whether the number of loci input to the analysis affected our results.

We created the G-PhoCS model by including two migration bands: one considering gene flow from *hoffmannsi* to *berlepschi* and one in the opposite direction, and we set the gamma distributed prior for migration rate per generation (m) constant across analyses ($\alpha = 0.002$, $\beta = 0.00001$) (Gronau et al. 2011; Bocalini et al. 2021). We also performed analyses using three sets of gamma-distributed priors for θ and τ ($(\alpha, \beta) = (1, 1, 000)$; $(1, 300)$; $(1, 100)$) (Gronau et al. 2011; Smith et al. 2014; Oswald et al. 2017; Bocalini et al. 2021) because we were interested in assessing how the choice of prior distributions affected estimates of divergence times and effective population sizes. Because we performed these three different analyses with two RAD datasets (6,000 and 10,000 loci), this resulted in a total of six G-PhoCS runs.

We ran the multi-threaded version of G-PhoCS for 1×10^6 iterations with 10% burn-in, sampling every 50 iterations. We used the “*find-finetunes TRUE*” option in the G-PhoCS control file to automatically fine-tune parameter estimates during burn-in, and we assessed MCMC convergence by examining ESS values in the program Tracer 1.6 (Rambaut et al. 2014), considering that the run converged when ESS values were ≥ 200 (Drummond et al. 2006). Finally, we converted estimates of θ and τ from mutations per site to effective numbers of individuals ($N_e = \theta/4\mu$) and divergence time in years ($T = \tau G/\mu$) using a mutation rate (μ) of 2.5×10^{-9} substitutions per site per generation (Nadachowska-Brzyska et al. 2015) and a generation time (G) of 2 years

(Johnson and Wolfe 2018). We calculated the average ancestral population size and the average divergence time across different G-PhoCS runs, and then we fed these values into the *momi2* models as detailed below. We used the average for parameter estimates, because the estimated values were consistent across different G-PhoCS runs.

After estimating ancestral population sizes and divergence times using G-PhoCS, we performed demographic inference using *momi2* (Moran Models for Inference) (Kamm et al. 2020) to identify the demographic model that best fit the observed data and to test whether a scenario of asymmetric introgression was supported by site frequency spectrum (SFS) patterns. We chose to estimate population parameters with G-PhoCS rather than with *momi2*, because G-PhoCS allows a posteriori estimation of absolute rather than relative parameters (Thom et al. 2020). We chose *momi2* to identify the best demographic scenario because it allowed us to test different models, whereas G-PhoCS assumes an isolation with migration model. For all demographic models, we used the function *momi.DemographicModel*, setting the ancestral effective population size to the average value obtained with G-PhoCS, the generation time as 2 years, and the mutations per generation as 2.5×10^{-9} , as mentioned above. We allowed all models to estimate current effective population sizes for *hoffmannsi* and *berlepschi*. We built 21 models with all possible combinations of the following states for (1) migration: no migration, one pulse of migration (set with the argument *add_pulse_param*), ongoing gene flow (more than three pulses of migration); (2) migration direction: migration from *hoffmannsi* to *berlepschi* (set with the option *move_lineages*), migration from *berlepschi* to *hoffmannsi*, and bidirectional migration; and (3) divergence time: *momi2* estimated time of divergence, estimated time of mitochondrial divergence (7×10^5 years, Ribas et al. 2018), time of divergence estimated by G-PhoCS (set with the option *add_time_param*). For models with more than one pulse of migration, we used a single class of pulse direction per model for simplicity.

To prepare the SFS input for each model, we used *tabix* 0.2.6 to compress and index the second SNP dataset that did not use the minor allele count filter. Then, we used a browser-extensible data (BED) file along with a population assignment file (Table S1) to produce an allele count file with the “*momi.read_vcf*” function, and we generated the SFS from the allele count file using the function “*momi.extract_sfs*”. We optimized models with the truncated Newton conjugate method (Gill and Murray 1974), performed 100 replicate runs per model, and selected the replicate run with the highest log-likelihood for input to the model selection procedure. We used the maximum likelihood (ML) for each model to compute the AICc, and we compared models using Δ AICc scores and Akaike weights (Burnham and Anderson 2002).

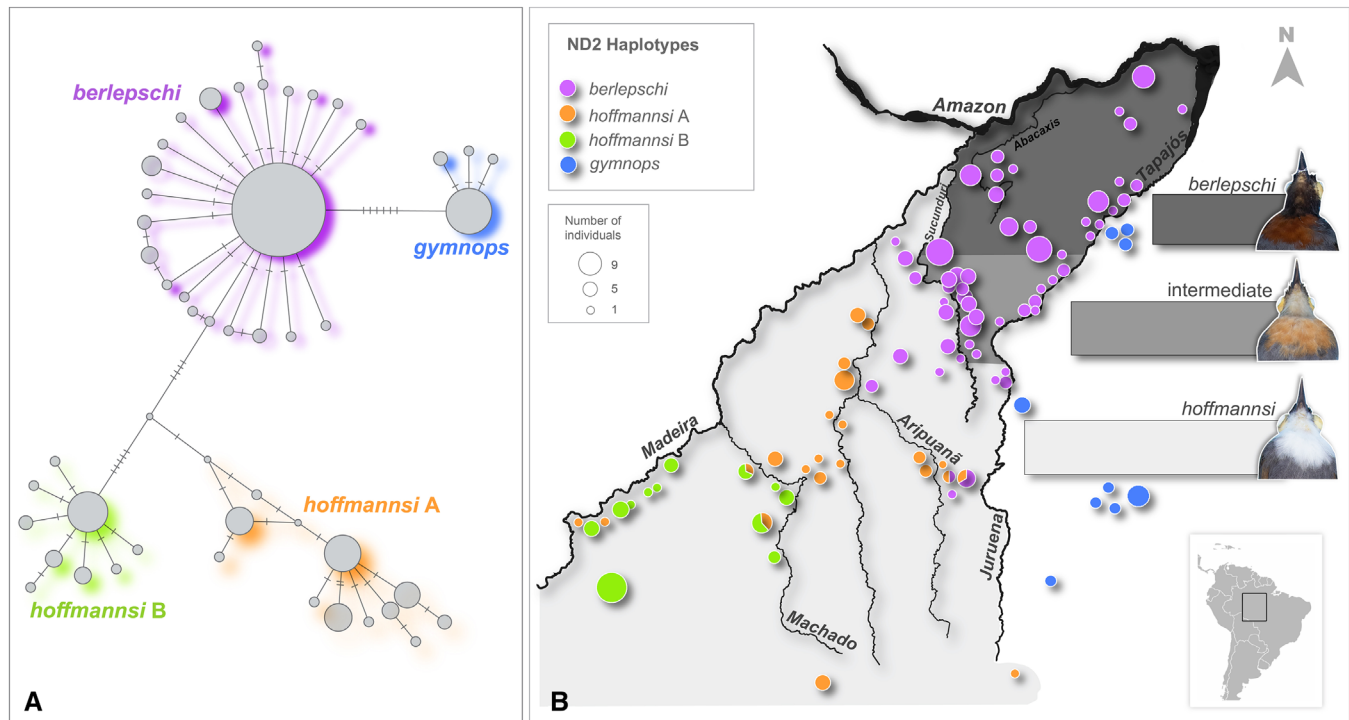


Figure 2. A single mitochondrial haplogroup (the *berlepschi* haplogroup) is found in the *Rhagmatorhina hoffmannsi* × *R. berlepschi* hybrid zone. (A) Three major haplogroups in the haplotype network of parental and hybrid zone populations, separated by four (*hoffmannsi* A vs. *berlepschi*), five (*hoffmannsi* A vs. *hoffmannsi* B), and nine (*hoffmannsi* B vs. *berlepschi*) substitutions at the ND2 gene. A fourth haplogroup, composed of *Rhagmatorhina gymnops* (an outgroup) samples in blue, is separated from the *berlepschi* haplogroup by six substitutions. (B) The four haplogroups depicted in panel A are delineated by rivers: the Machado (*hoffmannsi* A vs. *hoffmannsi* B), Aripuanã (*hoffmannsi* B vs. *berlepschi*), and Tapajós (*hoffmannsi* B and *berlepschi* vs. *gymnops*). Light gray shading represents the range of individuals with *hoffmannsi* chest color, medium gray represents the range of individuals with intermediate chest color, and dark gray represents the range of individuals with *berlepschi* chest color. Note that the location of the mitochondrial haplotype transition at the Aripuanã river does not coincide with the transition in plumage color.

Results

SUMMARY OF VARIATION IN MORPHOMETRIC CHARACTERS AND PLUMAGE COLOR

Based on gonad information and belly color, we identified the sex of individuals as male ($N = 119$; 54%), female ($N = 96$; 43%), or unknown ($N = 7$; 3%) (Table S1). We did not observe significant differences in any morphometric character between sexes of the same species or between the species ($P > 0.05$; Figs. S2 and S3). We found that throat and chest color differed significantly between *hoffmannsi* and *berlepschi* (Fig. S4). For downstream analyses, we pooled color measurements from male and female specimens after establishing that throat and chest color did not differ between sexes (Fig. S2; $P > 0.05$). As the metrics of chest and throat color, we used the percentage reflectance at 600 nm because this wavelength differed maximally between the species for these two traits (Fig. S4). From examining the plumage color of sampled individuals, we identified 115 specimens as phenotypically *hoffmannsi*, 73 as phenotypically *berlepschi*, and 34 as putatively recombinant.

MITOCHONDRIAL ANALYSES

The ND2 sequence data contained three major haplogroups (Figs. 2 and S5) that we refer to using the nomenclature of Ribas et al. (2018): (1) *hoffmannsi* B: occurring from the east bank of the Madeira River to the west bank of the Machado river and composed entirely of individuals with parental *hoffmannsi* plumage; (2) *hoffmannsi* A: occurring from the east bank of the Machado River to the west bank of the Aripuanã River and composed entirely of individuals with parental *hoffmannsi* plumage; and (3) *berlepschi*: occurring from the east bank of the Aripuanã River to the Amazon River and composed of individuals with parental *hoffmannsi* plumage, individuals with recombinant plumages, and individuals with parental *berlepschi* plumage. This nomenclature is somewhat confusing, so we emphasize here that the area occupied by the *berlepschi* haplogroup encompasses the entire *hoffmannsi* × *berlepschi* hybrid zone and that neither of the mitochondrial phylogeographic breaks were located where the plumage transition occurs between *hoffmannsi* and *berlepschi* (Fig. 2).

GENOME ASSEMBLY

Library sequencing by Dovetail produced 471 million read pairs for the short-insert library and 521 million read pairs for the Chicago library. After filtering contigs <1,000 bp, the Spades assembly included 109,564 contigs having an N50 of 18.7 kbp (L50 15,022). BESST scaffolding joined the Spades contigs into 49,853 scaffolds having an N50 of 51.4 kbp (L50 5347), and additional scaffolding with Chicago data followed by assembly polishing produced an intermediate assembly containing 19,412 scaffolds with an N50 of 318.5 kbp (L50 1050). The RaGOO pseudo-chromosomal assembly contained 8960 scaffolds, had an N50 of 72.8 Mbp (L50 5) and a total length of 1.07 Gbp. Length of pseudo-chromosome Z in our assembly was 75.8 Mbp (~100% of the *Chiroxiphia* Z chromosome) compared to 868 kbp (1.2% of the *Chiroxiphia* Z chromosome) for the Dove-tail assembly, and BUSCO results suggested that the pseudo-chromosomal assembly was more complete than the assembly produced by Dovetail (Table S3).

RAD SEQUENCING, VARIANT CALLING, AND VARIANT FILTRATION

Sequencing generated an average of 4.6×10^6 (95% CI = 4.3×10^6 to 4.8×10^6) reads per sample, and we mapped an average of 3.8×10^6 (CI = 3.6×10^6 to 4.0×10^6) unique, paired reads to the reference genome for each individual (Table S1). STACKS analysis produced a VCF file containing 132,457 SNPs that we reduced to 19,953 SNPs after filtering for coverage, minimum allele count, and SNPs with missing data. Additional filters for LD and heterozygote excess produced a final dataset containing 8,773 SNPs. The second SNP dataset that we used for demographic inference (with no minor allele filtering) included 20,427 SNPs.

From the set of 8,773 SNPs, we identified 24 diagnostic loci that differed in frequency by at least 60% (i.e., using the 0.80/0.20 cutoff) between parental samples of *hoffmannsi* and *berlepschi* (Table 2). Of the 24 SNPs, eight were Z-linked and 16 were autosomal. This number of diagnostic, Z-linked SNPs is greater than expected by chance. Assuming the Z chromosome is ~10% of the total genome, the probability that eight diagnostic SNPs would be Z-linked is 1×10^{-9} . The number of diagnostic SNPs decreased from 24 to 5 when we considered only those that differed by a frequency of 80% (i.e., using a 0.90/0.10 cutoff). Four of the five within this subset were Z-linked, and the probability of this proportion occurring by chance is 1×10^{-4} .

We observed few deviations from Hardy-Weinberg proportions. Some loci differed significantly in individual population samples, but there was no consistent pattern of deviation across diagnostic SNPs or population samples (Table S4).

POPULATION STRUCTURE INFERRED WITH RADseq DATA

sNMF and DAPC analyses indicated that sampled individuals were best represented by two genetic populations (Fig. S6). When we mapped ancestry coefficients for the best sNMF run ($\alpha = 100$, $k = 2$), we found that the location of intermediate individuals (ancestry coefficients ~ 0.3–0.6) was coincident with the location of the plumage color transition. Nuclear introgression extended 214 km along the transect southward into populations of *hoffmannsi* that showed no signs of plumage color introgression and 307 km northward into populations of *berlepschi* that showed no signs of plumage color introgression (Fig. 3).

In the triangle plot, most individuals were consistent with advanced generation hybrids and backcrosses. Two individuals were heterozygous at all five diagnostic SNPs and had an intermediate hybrid index, consistent with F1 hybrids (Fig. S7). Inspection of specimen vouchers revealed that one of the individuals (LSUMZ 73024) had the white chest and throat of *hoffmannsi*. The second individual (LSUMZ 86302) had a white chest with some brown feathers. Whether either of these plumages is consistent with an F1 hybrid is unclear because we do not know the dominance relationships of alleles underlying the plumage traits. The individual with intermediate plumage (LSUMZ 86302) could be an F1 if plumage inheritance is incompletely dominant.

GEOGRAPHIC CLINE ANALYSIS

We used HZAR to fit geographic clines to transitions in plumage color, mtDNA, the ancestry coefficient, and diagnostic SNPs across the hybrid zone (Tables 2 and S5; Fig. 4). We excluded diagnostic SNP8 entirely from further analysis because its cline was an outlier; the confidence limits of its width and cline center estimates fell well outside those of the other 23 diagnostic loci (Figs. S8 and S9). The size of cline center and cline width confidence limits increased linearly with cline width point estimates (Fig. 4C, D). In other words, as the width of a trait's cline increased, the confidence in its cline center and cline width point estimates decreased. This association was evident in a bivariate plot of width and center confidence intervals (Fig. S8). As the confidence interval for cline width narrowed, so did the confidence interval for cline center. Finally, we did not observe consistent differences in cline parameters between Z-linked and autosomal SNPs.

One of the most striking results of the geographic cline analysis was the statistically significant displacement of the mtDNA cline center from the centers of most other traits (Table 3). Discordance of cline centers was confirmed by composite likelihood analyses: $ML_{sum} = -1271$ and $ML_{comp} = -1399$ were significantly different ($P < 0.05$). The mtDNA cline was centered near the Aripuanã River, approximately 120 km south of the

Table 2. Parameters of geographic clines. Maximum likelihood cline widths (km) and cline centers (km), 95% confidence intervals inside parentheses. p_{\min} is the minimum estimated allele frequency at the *hoffmannsi* end of the cline, and p_{\max} is the maximum estimated frequency at the *berlepschi* end of the cline. Bold text indicates more stringent set of diagnostic SNPs (loci having an average allele frequency <0.1 at locality 1 and >0.9 at localities 20 and 21).

Traits	Chromosome	Chromosome position	Center (CI)	Width (CI)	p_{\min}	p_{\max}
mtDNA	–	–	–1 (–10/12)	42 (9/102)	–	–
Chest color	–	–	191 (179/205)	90 (4/136)	–	–
Throat color	–	–	203 (185/217)	97 (69/126)	–	–
Ancestry coefficient	–	–	120 (92/153)	454 (320/532)	–	–
SNP 1 (30853_133)	5	67229888	91 (45/133)	339 (236/465)	0	1
SNP 2 (38824_47)	Z	17227772	152 (89/214)	863 (642/1178)	0	1
SNP 3 (39205_23)	Z	26902159	113 (55/163)	292 (164/465)	0	1
SNP 4 (39402_114)	Z	30663389	224 (185/263)	470 (353/627)	0	1
SNP 5 (41066_95)	Z	66662725	203 (175/230)	296 (219/396)	0	1
SNP 6 (4214_7)	15	17823164	203 (175/230)	296 (219/396)	0	0.94
SNP 7 (13730_99)	25	5860813	250 (194/313)	775 (570/1066)	0	0.87
SNP 8 (14685_61)	2	114096992	–389 (–586/–255)	1189 (850/1734)	0	1
SNP 9 (15837_58)	2	31619537	65 (–40/161)	1441 (995/2196)	0	1
SNP 10 (16803_131)	2	49424972	36 (–39/105)	771 (545/1088)	0	1
SNP 11 (24097_117)	3	8767936	14 (–72/90)	1056 (777/1461)	0	1
SNP 12 (27090_85)	4	50044507	314 (240/406)	997 (708/1440)	0	1
SNP 13 (27729_36)	4	63830633	125 (44/203)	1141 (822/1624)	0	1
SNP 14 (28375_70)	5	15000651	142 (55/230)	1182 (821/1749)	0	1
SNP 15 (28535_53)	5	17999580	386 (318/475)	783 (559/1114)	0	1
SNP 16 (35063_64)	7	30354224	358 (283/459)	960 (678/1395)	0	1
SNP 17 (36065_51)	8	20785433	165 (45/360)	380 (83/886)	0	0.83
SNP 18 (38374_115)	scaffold_6391	1982	181 (108/258)	1059 (766/1499)	0	1
SNP 19 (38401_103)	scaffold_7264	3457	49 (–52/140)	1354 (952/2002)	0	1
SNP 20 (39223_60)	Z	27213976	354 (256/494)	1313 (888/2047)	0	1
SNP 21 (39293_59)	Z	28066173	159 (95/222)	882 (652/1208)	0	1
SNP 22 (40966_49)	Z	64970276	212 (169/260)	443 (292/643)	0	0.87
SNP 23 (41215_17)	Z	70780130	–30 (–105/35)	801 (610/1061)	0	1
SNP 24 (9844_78)	1	41140218	210 (135/290)	1077 (771/1534)	0	1

ancestry coefficient's cline center (Fig. 4E, F). Another striking result was the skewed variation in cline centers. Most cline centers were coincident with the center of the plumage color clines or occurred somewhere between the plumage color and mitochondrial cline centers. Only four loci (SNP12, SNP15, SNP16, and SNP20) showed the reverse pattern of a cline center displaced to the north of the plumage color cline. The majority of SNP cline centers occurring in between the centers of the mitochondrial and plumage clines is evident by a qualitative examination of the ancestry coefficient pie charts (Fig. 3). We also found that cline widths varied greatly among traits, suggesting a weak coupling effect (Fig. 4D).

NEUTRAL DIFFUSION

The expected cline width if secondary contact initiated 2,000 generations ago was ~225 km, which is narrower than all of the di-

agnostic SNP clines, suggesting that many of the nuclear markers are consistent with neutral diffusion (Table 2). In contrast, the mitochondrial cline was significantly narrower than expected under neutral diffusion (42 vs. ~225 km), suggesting it is being maintained by natural selection. In fact, for neutral diffusion to explain a cline width of 42 km, secondary contact must have begun 70 generations ago (i.e., ~140 years) (Johnson and Wolfe 2018). Historical specimens of *hoffmannsi* were collected ~50 years ago from the east bank of the Aripuanã River, suggesting that movement of the white plumage started at least 25 generations ago. Repeating the above analysis assuming initial contact 10,000 generations ago results in an expected cline width of 502 km. This expected cline width is consistent with cline widths of diagnostic nuclear loci. In sum, these results indicate neutral diffusion cannot be rejected for the diagnostic nuclear SNPs, and they also suggest natural selection could be maintaining the mitochondrial cline.

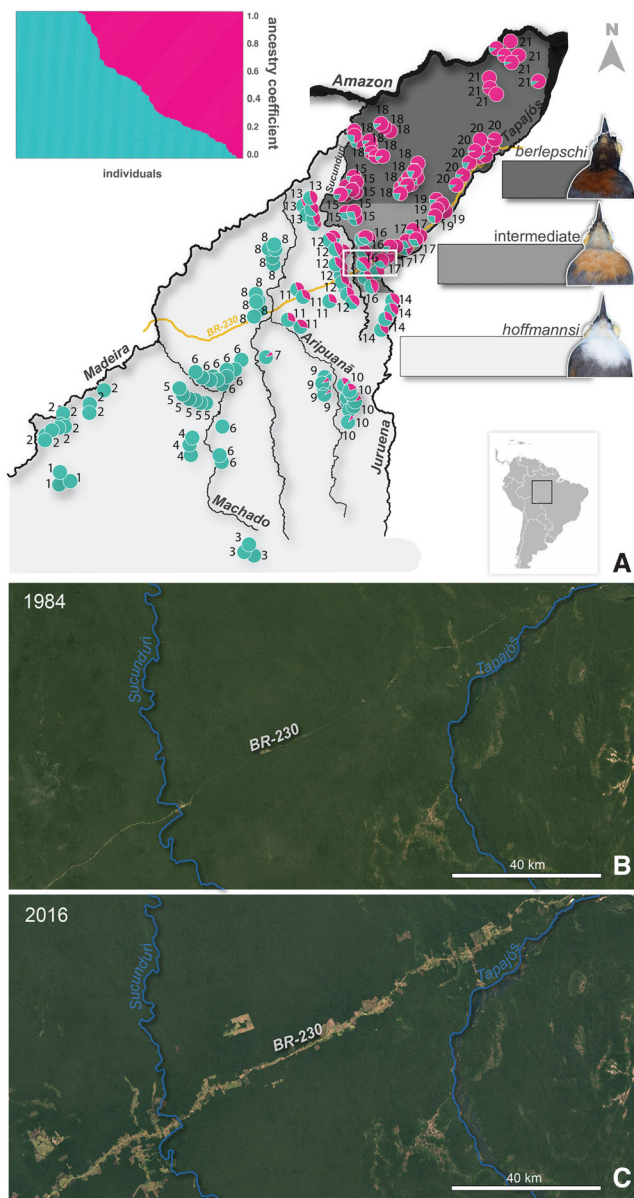


Figure 3. Plumage color and genetic ancestry of individuals across the *Rhegmatorhina hoffmannsi* × *R. berlepschi* hybrid zone. (A) Pie charts represent ancestry coefficients calculated from RAD-seq data (see inset sNMF admixture barplot). Pie-charts (main panel) and bars (inset panel) displaying both colors represent presumed admixed individuals. Light gray shading represents the range of individuals with *hoffmannsi* chest color, medium gray shading represents the range of individuals with intermediate chest color, and dark gray shading represents the range of individuals with *berlepschi* chest color. Trans-Amazonian Highway (BR-230) in yellow. Numbers indicate the transect population numbers. (B) Landsat imagery of the area within the white box in panel A showing forest extent close to the BR-230 highway during 1984. (C) Landsat imagery from 2016 showing the extent of deforestation along the BR-230 highway.

Table 3. Log-likelihood ratio test results for comparison of models where cline center is estimated and models in which cline center is fixed to be equal to the mitochondrial DNA cline center. *P*-values below 0.05 indicate significant differences between the log-likelihood of models with an estimated cline center and models with their cline center fixed to the center value of the mtDNA cline. Bold text indicates more stringent set of diagnostic SNPs (loci having an average allele frequency <0.1 at locality 1 and >0.9 at localities 20 and 21). Italics indicate *P* < 0.05.

Traits	Log-likelihood best model	Log-likelihood fixed center (−10 to 12 km)	Likelihood ratio test <i>P</i> -value
Chest color	−510	−619	<0.05
Throat color	−559	−587	<0.05
Ancestry coefficient	−2.3	−62.7	<0.05
SNP 1 (30853_133)	−9.2	−13.7	<0.05
SNP 2 (38824_47)	−9.3	−15.5	<0.05
SNP 3 (39205_23)	−6.8	−11.0	<0.05
SNP 4 (39402_114)	−12.2	−36.4	<0.05
SNP 5 (41066_95)	−14.2	−43.5	<0.05
SNP 6 (4214_7)	−6.5	−18.4	<0.05
SNP 7 (13730_99)	−10.7	−28.6	<0.05
SNP 8 (14685_61)	−9.3	−30.4	<0.05
SNP 9 (15837_58)	−5.6	−6.2	0.25
SNP 10 (16803_131)	−6.7	−7.0	0.44
SNP 11 (24097_117)	−5.2	−5.2	1.00
SNP 12 (27090_85)	−8.4	−28.4	<0.05
SNP 13 (27729_36)	−11.4	−14.3	<0.05
SNP 14 (28375_70)	−13.0	−16.3	<0.05
SNP 15 (28535_53)	−3.7	−41.1	<0.05
SNP 16 (35063_64)	−5.3	−31.7	<0.05
SNP 17 (36065_51)	−5.7	−6.8	0.13
SNP 18 (38374_115)	−6.3	−12.8	<0.05
SNP 19 (38401_103)	−6.9	−7.3	0.37
SNP 20 (39223_60)	−7.6	−25.0	<0.05
SNP 21 (39293_59)	−13.2	−19.7	<0.05
SNP 22 (40966_49)	−7.2	−26.0	<0.05
SNP 23 (41215_17)	−14.1	−14.1	1.00
SNP 24 (9844_78)	−6.0	−14.7	<0.05

GENOMIC CLINES

Of the 24 diagnostic SNPs, we found that seven could not have their ancestry assigned to either *hoffmannsi* or *berlepschi* ($v_i = 0$) by genomic cline analysis. Of the remaining 17 diagnostic loci, only Z-linked SNP5 had a genomic cline that was significantly different from the null model ($u_i = 1.43$; $P < 0.01$; Fig. 5), indicating that it may be under selection (Table S6). SNP5 has *hoffmannsi* ancestry but occurs within the genomic background of *berlepschi*, it was one of the high-confidence markers in the geographic cline analysis, and its center was displaced significantly

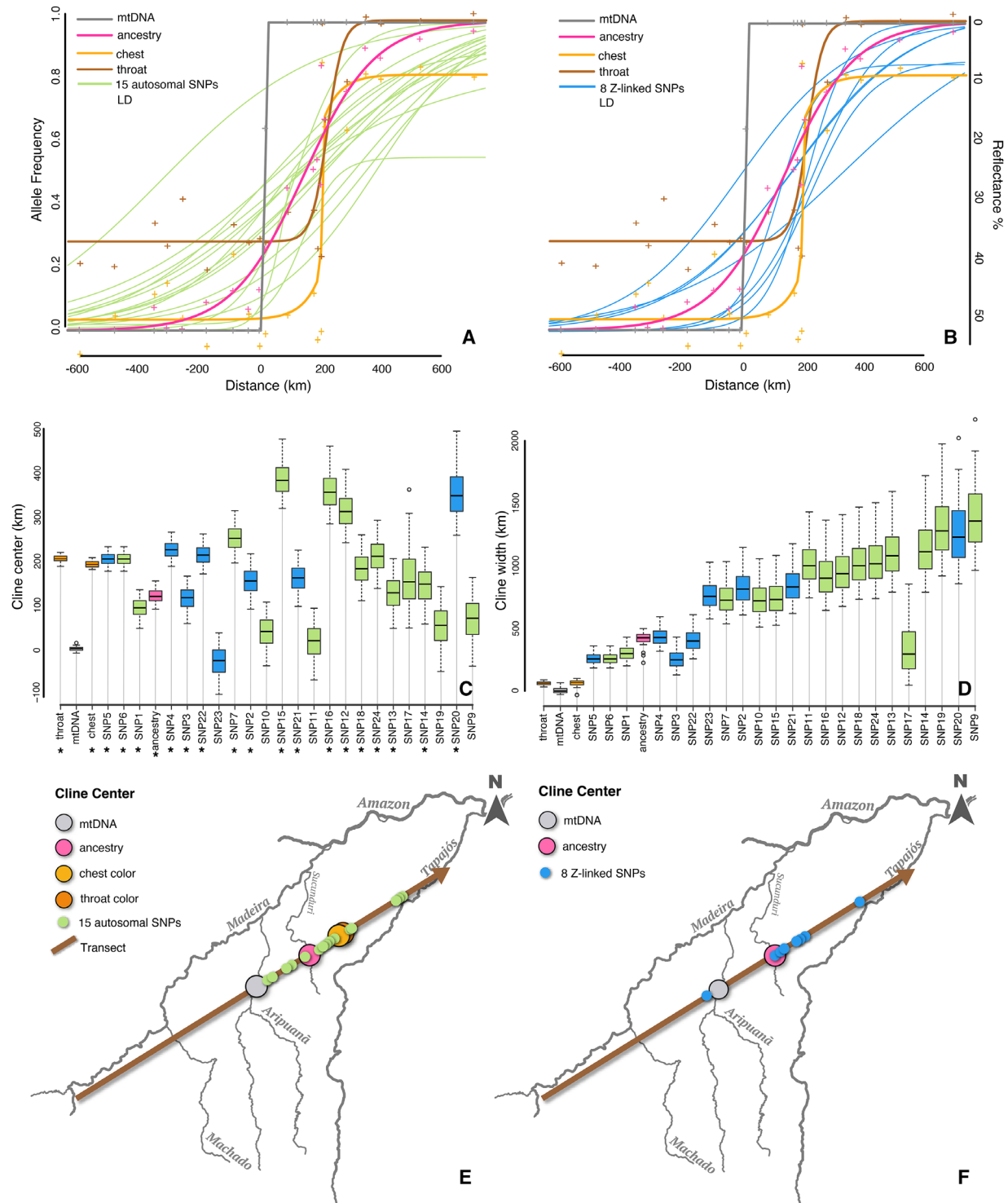


Figure 4. Geographic cline analysis. (A) Distance indicates position along the transect, where 0 km is the point that crosses the Aripuanã River. The cline for the ancestry coefficient is represented by the pink line, for chest color by the orange line, for throat color by the brown line, for mtDNA by the gray line, and the clines for 15 autosomal SNPs by the green lines. (B) Same as in panel A, except the eight Z-linked, diagnostic SNPs are represented by blue lines. (C) Boxplots of maximum-likelihood cline center estimates and 95% confidence intervals, sorted by sizes of cline center confidence intervals. Boxplot colors correspond to cline colors in panels A and B. Asterisks below horizontal-axis labels indicate cline centers significantly shifted from the cline center estimated for mtDNA. (D) Box plots of maximum-likelihood cline width estimates and 95% confidence intervals, sorted by sizes of cline width confidence intervals. (E) Geographic position of cline centers for mtDNA, ancestry coefficient, chest/throat plumage reflectance, and autosomal SNPs along the transect. (F) Geographic position of cline centers for eight Z-linked, diagnostic SNPs along the transect.

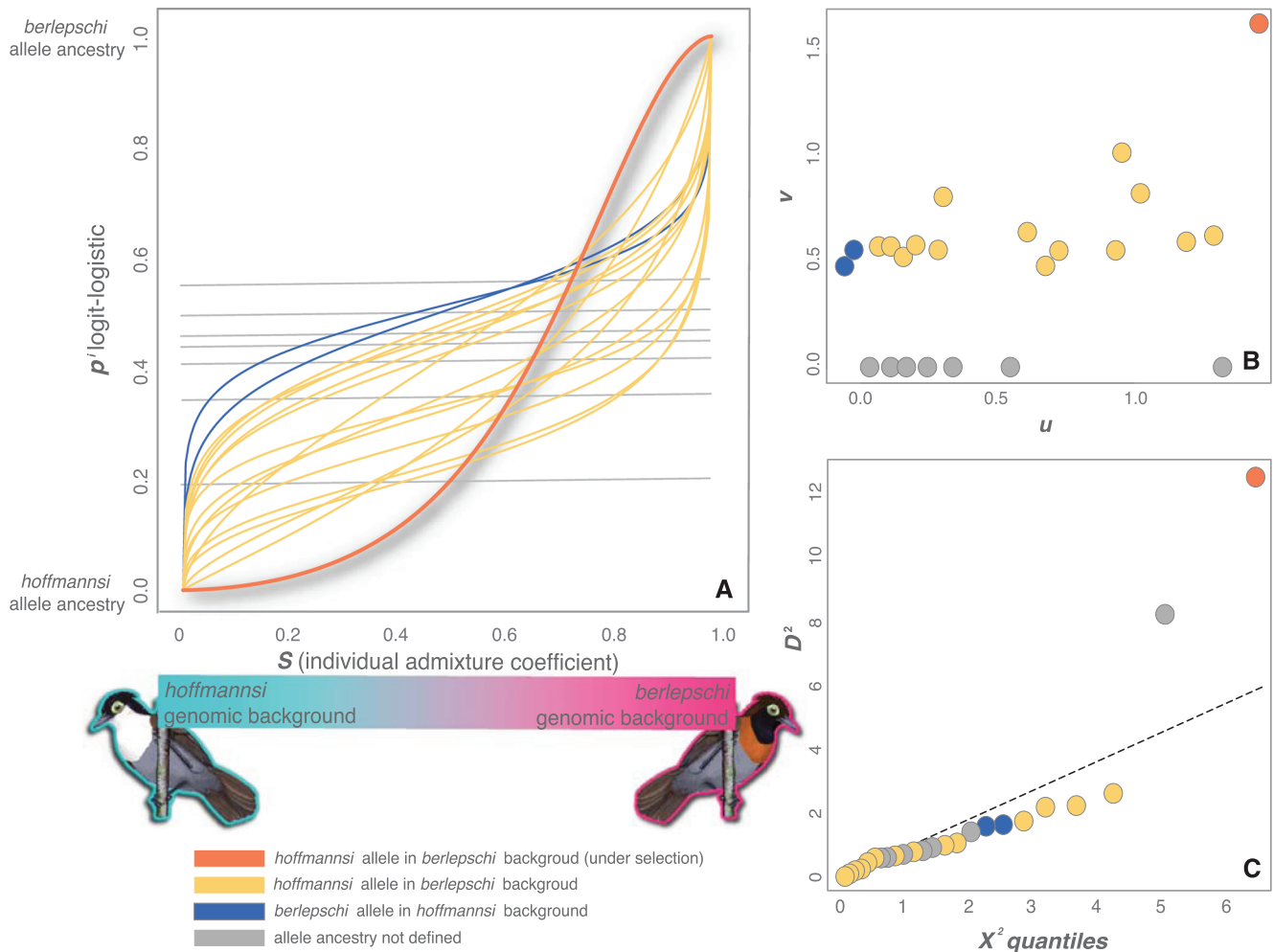


Figure 5. Genomic clines indicate introgression of 15 alleles with *hoffmannsi* ancestry into the *berlepschi* genomic background. (A) The X-axis represents the value of S , which can be interpreted as the probable ancestry of each individual's genomic background. The Y-axis represents the logit logistic, where p_i is the proportion of copies of locus i inherited from one of the target populations (here *berlepschi*). The gray lines represent seven SNPs whose ancestry could not be identified. Blue lines represent two alleles with *berlepschi* ancestry introgressed into the *hoffmannsi* genomic background. Yellow lines and the orange line represent 15 alleles with *hoffmannsi* ancestry introgressed into the *berlepschi* genomic background. The orange line represents Z-linked SNP5, the only diagnostic locus with a genomic cline significantly different from the null cline, suggesting it may be under selection. (B) v indicates the slope of p_i , and u indicates the relative difference in cline position relative to the inflection point. SNPs with v values equal to zero did not have their ancestry identified (gray circles), SNPs with negative values of u have *berlepschi* alleles but are on the genomic background of *hoffmannsi* (blue circles), and SNPs with positive u values have *hoffmannsi* ancestry but are on the genomic background of *berlepschi* (yellow and orange circles). The orange circle represents Z-linked SNP5. (C) Plot showing the squared Mahalanobis distance D^2 of each SNP, against the expected χ^2 distribution. A locus (SNP5, in orange) with D^2 greater than expected and visually deviating from quantile-quantile plot is considered an outlier and could be under selection. *Rhegmatorhina* illustrations by GDR.

north of the mtDNA cline center, along with several other nuclear clines.

DEMOGRAPHIC ANALYSIS OF SNP DATA

Estimates of ancestral effective population size were consistent across G-PhoCS runs with different priors and input datasets ($\hat{\theta} = 1,600,000 \pm 7100$ individuals), whereas estimates of divergence time were more variable ($\hat{\tau} = 72,000 \pm 11,000$ years) (Table S7)

and an order of magnitude younger than previous mitochondrial estimates of divergence time (Ribas et al. 2018). Model comparisons suggested the best fit model: (1) estimated the time of divergence, as opposed to accepting the divergence time estimated by G-PhoCS or the one presented in Ribas et al. (2018); (2) included ongoing migration, rather than one single pulse of migration or an absence of migration; and (3) included unidirectional migration from *berlepschi* to *hoffmannsi*, a pattern

consistent with *hoffmannsi* being the invader species over the local *berlepschi* (Currat et al. 2008) (Table S8).

Discussion

The mitochondrial, nuclear, and plumage color patterns we characterized in *Rhegmatorhina* suggest that, after secondary contact in the vicinity of the Aripuanã River where the mitochondrial transition occurs, the majority of traits and loci experienced a net northward movement, with most clines currently centered in a narrow band of habitat between the Sucunduri and Tapajós Rivers. This interpretation is based on significant displacement of the mitochondrial cline from most other clines, including plumage color, and by the greater net introgression of *berlepschi* nuclear alleles into the genomic background of *hoffmannsi*—the expected pattern if *hoffmannsi* is the invader and *berlepschi* the invadée (Figs. 3 and 4; Currat et al. 2008). It is possible that the current geographic position of the nuclear and phenotypic hybrid zone is stabilized by a habitat bottleneck created by the narrow forest corridor between the Sucunduri River and the Tapajós and Juruena Rivers (Fig. 3).

If the hybrid zone is moving northward, one eventual outcome, barring anthropogenic effects and assuming its position is not fully stabilized by the geographic bottleneck described above, would be extinction of *berlepschi* via genetic swamping. However, significant habitat degradation in this region is altering the natural processes operating in the hybrid zone, most significantly the construction of highway BR-230 during the 1960s and 1970s. Also known as the Trans-Amazonian Highway, BR-230 bisects the hybrid zone precisely in the narrow band of habitat where most nuclear clines are centered and where phenotypic intermediates occur (Fig. 3). Until relatively recently, habitable forest still occurred along the highway in this region that would have allowed antbirds to cross. This is no longer the case. We speculate that dispersal across BR-230 is now greatly diminished, at best. Additional data are needed to directly examine the influence of BR-230 on bird densities and dispersal, as well as on the *Eciton* army ants followed by the birds, but it seems clear that the future of the hybrid zone will now be determined in part by BR-230.

In terms of evolutionary forces, the narrowness of the mitochondrial cline makes it likely that natural selection is playing a significant role in its maintenance, but we cannot reject neutral diffusion in explaining the wider nuclear clines. Nonetheless, there is some evidence for reduced hybrid fitness in the nuclear genome. For example, the disproportionate number of Z-linked diagnostic SNPs could indicate greater selection against females (the heterogametic sex in birds) in accordance with Haldane's Rule (Carling and Brumfield 2008). Below we examine some of the major patterns in the *Rhegmatorhina* hybrid zone, explore

some potential causes of these patterns, and propose hypotheses to be tested in future work.

DISPLACEMENT OF MITOCHONDRIAL AND NUCLEAR CLINES

We found that the center of the mitochondrial cline near the Aripuanã River was displaced significantly from the center of the clines for plumage color and most nuclear loci (Fig. 4). Empirical examples of hybrid zones in which mitochondrial and nuclear/phenotypic clines are displaced from one another are relatively abundant in the literature (summarized in Toews and Brelsford 2012). One hypothesis for the discordance we cannot reject is that the mitochondrial gene we sampled (ND2) evolves too slowly to exhibit sequence divergence between the two species. It could be that sampling of more rapidly evolving mitochondrial genes would reveal mitochondrial divergence in the same geographic location as the SNP and phenotypic transitions. This would be unusual, because it would imply that the mitochondrial divergence we observed within *hoffmannsi* across the nearby Aripuanã occurred without any accompanying nuclear or phenotypic divergence. However, the SNP data suggested the species divergence could have been very recent (70,000 ya), in which case it would not be unusual to see little, if any, mitochondrial divergence. Assuming the displacement is real, three other hypotheses proposed to explain displaced mitochondrial and nuclear geographic clines in vertebrates are genetic drift, adaptive introgression of mtDNA, and mtDNA of one lineage left behind following movement of the hybrid zone (Currat et al. 2008).

The genetic drift hypothesis suggests that some proportion of the among-locus variance in geographic cline centers is due to sampling error and genetic drift. Both factors certainly account for a proportion of the among-trait variance we observed in cline centers and widths. Whether drift alone could account for the displaced mitochondrial cline is unclear, but it is plausible given the smaller effective population size of mitochondrial loci (Nei and Tajima 1981). For example, initial secondary contact between *hoffmannsi* and *berlepschi* could have been at the Sucunduri River, the site of the current transition zone between the two plumage types. Genetic drift in the hybrid zone could have led to the fixation of the *berlepschi* haplotype west of the Sucunduri. We cannot reject this possibility, but it seems less likely given the essential cytonuclear associations often found in species (Hill 2019).

The adaptive introgression hypothesis proposes that one of the two mitochondrial haplotypes is selectively advantageous in both species (Toews et al. 2014). For *Rhegmatorhina*, this would suggest the *berlepschi* mitochondrial haplogroup crossed the nuclear hybrid zone and introgressed southward as far as the mitochondrial break near the Aripuanã River. This seems unlikely based on Haldane's rule in which reduced hybrid fitness is usually

more pronounced in the heterogametic sex. Because females are the heterogametic sex in birds, this effect would also limit the introgression of the matrilineally inherited mitochondrion. In terms of the *berlepschi* haplotype spreading due to a selective advantage, we have no way to directly measure the fitness of different mitochondrial haplotypes and thus cannot evaluate this hypothesis. However, there are no obvious thermal or other gradients in this region that would be a selection gradient. Moreover, studies that have modeled the expansion of advantageous genes across hybrid zones show that they spread to fixation extremely rapidly (Piálek and Barton 1997). If so, then the mitochondrial haplotype should have spread throughout the distribution of *hoffmannsi*, but we only observed it as far as the Aripuanã River. One potential explanation for its lack of further spread would be if birds are unable to circumnavigate the Aripuanã, either due to the river itself or to inhospitable habitat at its headwaters. This is something we plan to explore in future work, but the presence of *hoffmannsi* on both banks indicates the Aripuanã River was circumnavigable at some point in the past, which would have provided an opportunity for an advantageous haplotype to progress. In sum, we cannot reject an adaptive mitochondrial explanation, but it seems unlikely. More sampling in the headwaters of the Aripuanã is needed, as are studies of mitochondrial function in the different haplotypes.

In a third hypothesis, the mtDNA of one haplogroup, in our case *hoffmannsi* A, failed to accompany the northward-moving nuclear hybrid zone (Gyllensten and Wilson 1987) leading to displaced mitochondrial and nuclear clines. As with most hybrid zones, the exact mechanism by which this displacement would have occurred is unknown but it could be due to an asymmetry in fitness that results in only one of the two mitochondrial haplotypes being passed on to hybrids. Differential inheritance of mitochondrial haplotypes could occur by prezygotic mechanisms that result in unidirectional hybridization or by a postzygotic mechanism in which hybridization is reciprocal but the offspring's viability or fertility is not (Wirtz 1999).

There are no studies addressing the prevalence of prezygotic barriers in *Rhegmatorhina*. Because many aspects of the biology of *hoffmannsi* and *berlepschi*, with the exception of plumage color, are essentially indistinguishable between the two species (Willis 1969), plumage color would be the putative factor influencing assortative mating. Instead of a strong prezygotic barrier, our results could indicate a skewed preference for individuals with white plumage. For example, in lekking *Manacus* manakins, skewed mating success of yellow males may result in a bias toward hybridization between females of the white species (White-collared Manakins, *Manacus candei*) and males of the Golden-collared Manakins (*Manacus vitellinus*) at leks in western Panama (Stein and Uy 2006). In *Rhegmatorhina*, if matings with individuals having white plumage are more frequent than with individuals having a black throat and brown chest,

it is expected that the white plumage of *hoffmannsi* would become more prevalent, supplanting dark individuals in the original range of *berlepschi*. Alternatively, the northward advance of white plumage could reflect genetic dominance of the alleles responsible for the white phenotype over the alleles promoting the alternative plumage colors (Semenov et al. 2021). This idea could be tested if the loci and alleles responsible for plumage color were known. Although preference for the white plumage and dominance could explain a northward movement of *hoffmannsi* white plumage color, the two mechanisms fail to explain why the *hoffmannsi* mitochondrial haplotype would not “accompany” the plumage color movement.

Mechanisms also exist that would produce, in the early stages of secondary contact, offspring that only have one of the two mitochondria represented, but it is difficult to envision this pattern persisting into later generations. For example, if initial secondary contact was restricted to a few *hoffmannsi* males that circumnavigated the Aripuanã into the distribution of *berlepschi*, then all hybrids, at least initially, would have the *berlepschi* haplotype. The problem is that this scenario of *berlepschi* haplotypes in hybrid offspring would break down when female *hoffmannsi* eventually circumnavigated the river and hybridized with *berlepschi*. The hypothesis also seems less likely because female birds generally tend to disperse greater distances than males (Greenwood 1980). If anything, it would be *hoffmannsi* females that first colonized the east bank of the Aripuanã. This would have resulted in the *hoffmannsi* A haplogroup on the east bank of the Aripuanã. Low levels of movement across the Aripuanã are possible. To date, we have observed three *hoffmannsi* A individuals on the right bank of the Aripuanã (two females and one male), all at its narrow headwaters (Fig. 2).

A postzygotic mechanism, and a cytonuclear incompatibility in particular, seems like a plausible hypothesis to explain the displaced clines we observed in *Rhegmatorhina*. Empirical studies of avian hybridization have demonstrated negative, female-biased fitness effects such as inviability and infertility, in accordance with Haldane's rule (Carling and Brumfield 2008; Gowen et al. 2014). Detrimental fitness effects experienced by females extend to the mitochondrial genome, as well as to any nuclear genes that are linked epistatically to the mitochondrion. In *Rhegmatorhina*, the discordance we observed could be explained if females are inviable or infertile when they have the *berlepschi* mitochondrial haplogroup and an unknown Z-linked or autosomal *hoffmannsi* allele(s) (Dasmahapatra et al. 2002; Mishmar et al. 2003). If the fitness reductions were only partial inviability or partial infertility, then the mitochondrial cline we observed would not have been so narrow. We predict that the unknown *hoffmannsi* nuclear allele(s) should also have its cline centered near the Aripuanã River. Among the diagnostic SNPs we identified, the geographic clines of several are statistically concordant with

the mtDNA cline, yet their cline widths are much wider than the mtDNA cline, suggesting these nuclear loci are not involved directly in mitonuclear incompatibilities (Fig. 4C, D). The details of a putative cytonuclear interaction are currently unknown to us, but they are the subject of ongoing work.

MOVING HYBRID ZONE

After secondary contact, which we assume occurred somewhere in the vicinity of the Aripuanã River, the plumage traits and nuclear loci, excepting any nuclear gene(s) involved in a putative cytonuclear interaction, moved northward to their current positions in the narrow band of habitat between the Sucunduri River and the Tapajós/Juruena Rivers (Fig. 3). Viewed from the perspective of a biological invasion with hybridization and assuming *hoffmannsi* is the invader and *berlepschi* the invadée, the geographic structuring of genetic variation, including the unidirectional migration from *berlepschi* to *hoffmannsi* indicated by the SFS, is consistent with expectations (Currat et al. 2008): a greater geographic extent of *berlepschi* introgression into *hoffmannsi* (Fig. 3). Alternatively, the *berlepschi* nuclear alleles found between the Aripuanã and Sucunduri Rivers could be interpreted as a genetic wake left behind the northward-moving hybrid zone (Rohwer et al. 2001) or they could be viewed as ancestral alleles that have been retained. The retention hypothesis seems unlikely given the decay of *berlepschi* alleles moving southward from the hybrid zone, but the genetic wake hypothesis is a plausible explanation for the presence of some alleles. Finally, there may be a more complicated history of hybridization that is difficult to disentangle from extant patterns of diversity (Wang et al. 2019).

The ideal corroborating data to support a moving hybrid zone would be direct observations of historical specimens in putative invaded areas. For example, Wang et al. (2019) used samples collected 30 years apart to assess hybrid zone movements in the *Setophaga occidentalis/townsendi* hybrid zone. Unfortunately, there are no census data or specimens from the *Rhegmatorhina* hybrid zone that we could use to directly assess past movements. Seven individuals of parental *hoffmannsi* collected in 1971 from the east bank of the Aripuanã are some of the very few historical specimens from the region (MZUSP 62285, 62286, 62287, 62288, 62293, 62294, and 62295), and these are consistent with the modern phenotypic structure of the hybrid zone.

The Aripuanã River is well known as a site of taxon turnover (Cohn-Haft et al. 2007), and mitochondrial studies that examined the phylogeographic structure of understory birds in this region have all found mitochondrial breaks of varying ages between populations from its opposite banks, including in *Glyphorhynchus spirurus* (Fernandes et al. 2013), *Thamnophilus aethiops* (Thom and Aleixo 2015), *Hypocnemis rondoni* (Fernandes et al. 2014), and *Lepidothrix nattereri* (Dias et al. 2018). Several avian taxon pairs also turnover across the Sucunduri River (Fernandes 2013;

Whitney et al. 2013; Schultz et al. 2019), but the *Rhegmatorhina* hybrid zone is the only one of these turnovers that has been analyzed. The occurrence of multiple contact zones within the Madeira/Tapajós interfluvium suggests a dynamic system that provides a natural laboratory to study the outcomes of secondary contact.

AUTHOR CONTRIBUTIONS

GDR, MAR, BMW, FS, LFS, BCF, and RTB conceived the study and wrote the manuscript. GDR, MAR, BMW, FS, and LFS performed field work from 2004 to 2019. GDR collected laboratory data. GDR collected museum specimen data. GDR and BCF conducted analyses. GDR made figures.

ACKNOWLEDGMENTS

The authors thank the editors B. Emerson and A. McAdam and two anonymous referees for their comments and suggestions, all of which improved this manuscript. The authors thank C. Ribas, M. Cohn-haft, G. Lima (INPA), A. Aleixo, F. Lima (MPEG), S. Hackett, J. Bates, and B. Marks (FMNH), D. Dittmann (LSU), and C. Miyaki (University of São Paulo) for providing valuable loans of tissues and for opening the doors of their bird collections and laboratories to GDR. The authors are thankful for all the volunteers that helped with *Rhegmatorhina* fieldwork over the course of more than nine LSU-MZUSP expeditions, and the authors are especially grateful to D. Schmitt, G. Schmitt, T. Jackson, M. Lima, P. Balduino, M. Félix, I. Jean and F. Arantes. The authors thank E. Duval and the Manakin Genomics Research Coordination Network (DBI-1457541) for making the *Chiroxiptia* genome assembly available through NCBI. The authors thank J. Salter, C. Oliveros, A. Schoonmaker, R. Beco, F. Bocalini, S. Bolívar, and J. Battilana for helping with laboratory work. The authors thank B. Fitzpatrick for insightful discussions about genomic clines. The authors thank I. Gronau, M. Hickerson, and Y. Song for discussions about demographic inference and introgression direction. F. Alda, G. Bravo and R. Marcondes provided helpful comments on an earlier version of the manuscript. Portions of this research were conducted with high-performance computing resources provided by Louisiana State University (<http://www.hpc.lsu.edu>) and Louisiana Optical Network Infrastructure (<http://www.loni.org>). Financial support was provided by the National Science Foundation (DEB-1146265, DEB-1655624), Coypu Foundation, CNPq (2014/2009-1), American Association of University Women, AMNH Chapman Memorial Fund, LSU Alumni Association, startup funds from LSU to BCF, Society of Systematic Biologists, Scientific Exploration Society, and Wilson Ornithological Society.

DATA ARCHIVING

Raw read data used for genome assembly are available from National Center for Biotechnology Information (NCBI) BioProject PRJNA545868. This Whole Genome Shotgun project has been deposited at DDBJ/ENA/GenBank under the accession VZSN000000000, and the version described in this article (the RaGOO pseudo-chromosomal assembly) is VZSN02000000 (NCBI PRJNA669390). RAD sequencing data and ND2 sequences are available from BioProject PRJNA763942.

CONFLICT OF INTEREST

The authors declare no conflict of interest.

LITERATURE CITED

- Alonge, M., S. Soyk, S. Ramakrishnan, X. Wang, S. Goodwin, F. J. Sedlazeck, Z. B. Lippman, and M. C. Schatz. 2019. Fast and accurate reference-guided scaffolding of draft genomes. *Genome Biol.* 20:1–17.
- Altschul, S. F., W. Gish, W. Miller, E. W. Myers, and D. J. Lipman. 1990. Basic Local Alignment Search Tool 2. *J. Mol. Biol.* 215:403–410.
- Backenroth, D., and S. Carmi. 2019. A test for deviations from expected genotype frequencies on the X chromosome for sex-biased admixed populations. *Heredity* 123:470–478.
- Baird, N. A., P. D. Etter, T. S. Atwood, M. C. Currey, A. L. Shiver, Z. A. Lewis, E. U. Selker, W. A. Cresko, and E. A. Johnson. 2008. Rapid SNP discovery and genetic mapping using sequenced RAD markers. *PLoS ONE* 3:1–7.
- Barton, N. H. 2008. The effect of a barrier to gene flow on patterns of geographic variation. *Genet. Res.* 90:139–149.
- Barton, N. H., and K. S. Gale. 1993. Genetic analysis of hybrid zones. Pp. 13–45 in R. G. Harrison, ed. *Hybrid zones and the evolutionary process*. Oxford Univ. Press, New York.
- Bayona-Vásquez, N. J., T. C. Glenn, T. J. Kieran, T. W. Pierson, S. L. Hoffberg, P. A. Scott, K. E. Bentley, J. W. Finger, S. Louha, N. Troendle, et al. 2019. Adapterama III: quadruple-indexed, double/triple-enzyme RADseq libraries (2RAD/3RAD). *PeerJ* 2019:1–25.
- Bazykin, A. D. 1969. Hypothetical mechanism of speciation. *Evolution* 23:685–687.
- Bocalini, F., S. D. Bolívar-Leguizamón, L. F. Silveira, and G. A. Bravo. 2021. Comparative phylogeographic and demographic analyses reveal a congruent pattern of sister relationships between bird populations of the northern and south-central Atlantic Forest. *Mol. Phylogenet. Evol.* 154:106973.
- Bolger, A. M., M. Lohse, and B. Usadel. 2014. Trimmomatic: a flexible trimmer for Illumina sequence data. *Bioinformatics* 30:2114–2120.
- Bouckaert, R., J. Heled, D. Kuhnert, T. Vaughan, C.-H. Wu, D. Xie, M. A. Suchard, A. Rambaut, and A. J. Drummond. 2014. BEAST2: a software platform for Bayesian evolutionary analysis. *PLoS Comput. Biol.* 10:e1003537.
- Bronson, C. L., T. C. Grubb, G. D. Sattler, and M. J. Braun. 2005. Reproductive success across the Black-capped Chickadee (*Poecile atricapillus*) and Carolina Chickadee (*P. carolinensis*) hybrid zone in Ohio. *Auk* 122:759–772.
- Burnham, K. P., and D. R. Anderson. 2002. *Model selection and multimodel inference: a practical information-theoretic approach*. Springer, New York.
- Butlin, R. K., and C. M. Smadja. 2018. Coupling, reinforcement, and speciation. *Am. Nat.* 191:155–172.
- Carling, M. D., and R. T. Brumfield. 2008. Haldane's rule in an avian system: using cline theory and divergence population genetics to test for differential introgression of mitochondrial, autosomal, and sex-linked loci across the *Passerina* bunting hybrid zone. *Evolution* 62:2600–2615.
- Catchen, J., P. A. Hohenlohe, S. Bassham, A. Amores, and W. A. Cresko. 2013. Stacks: an analysis tool set for population genomics. *Mol. Ecol.* 22:3124–3140.
- Chang, C. C., C. C. Chow, L. C. A. M. Tellier, S. Vattikuti, S. M. Purcell, and J. J. Lee. 2015. Second-generation PLINK: rising to the challenge of larger and richer datasets. *Gigascience* 4:1–16.
- Chattopadhyay, B., K. M. Garg, and U. Ramakrishnan. 2014. Effect of diversity and missing data on genetic assignment with RAD-seq markers. *BMC Res. Notes* 7:4–6.
- Chen, B., J. W. Cole, and C. Grond-Ginsbach. 2017. Departure from Hardy-Weinberg Equilibrium and genotyping error. *Front. Genet.* 8:1–6.
- Clement, M., Q. Snell, P. Walke, D. Posada, and K. Crandall. 2002. TCS: estimating gene genealogies. P. 184 in *Proceedings of the 16th International Symposium on Parallel and Distributed Processing*. IEEE, Piscataway, NJ.
- Cohn-Haft, M., A. M. F. Pacheco, C. L. Bechtoldt, M. F. N. M. Torres, A. M. Fernandes, C. H. Sardelli, and I. T. Macêdo. 2007. Inventário ornitológico. Pp. 145–178 in D. Rapp Py, ed. *Biodiversidade do Médio Madeira: base científicas para propostas de conservação*. INPA, Manaus, Brazil.
- Cronemberger, Á., A. Aleixo, E. Mikkelsen, and J. Weir. 2020. Postzygotic isolation drives genomic speciation between highly cryptic *Hypocnemis* antbirds from Amazonia. *Evolution* 5:1689–1699.
- Currat, M., M. Ruedi, R. J. Petit, and L. Excoffier. 2008. The hidden side of invasions: massive introgression by local genes. *Evolution* 62:1908–1920.
- Danecek, P., A. Auton, G. Abecasis, C. A. Albers, E. Banks, M. A. DePristo, R. E. Handsaker, G. Lunter, G. T. Marth, S. T. Sherry, et al. 2011. The variant call format and VCFtools. *Bioinformatics* 27:2156–2158.
- Dasmahapatra, K. K., M. J. Blum, A. Aiello, S. Hackwel, N. Davies, E. P. Bermingham, and J. Mallet. 2002. Inferences from a rapidly moving hybrid zone. *Evolution* 56:741–753.
- Derryberry, E. P., G. E. Derryberry, J. M. Maley, and R. T. Brumfield. 2014. HZAR: hybrid zone analysis using an R software package. *Mol. Ecol. Resour.* 14:652–663.
- Dias, C., K. de A Lima, J. Araripe, A. Aleixo, M. Vallinoto, I. Sampaio, H. Schneider, and P. S. do Rêgo. 2018. Mitochondrial introgression obscures phylogenetic relationships among manakins of the genus *Lepidothrix* (Aves: Pipridae). *Mol. Phylogenet. Evol.* 126:314–320.
- Drummond, A. J., S. Y. W. Ho, M. J. Phillips, and A. Rambaut. 2006. Relaxed phylogenetics and dating with confidence. *PLoS Biol.* 4:699–710.
- Edgar, R. C. 2004. MUSCLE: multiple sequence alignment with high accuracy and high throughput. *Nucleic Acids Res.* 32:1792–1797.
- Endler, J. A. 1977. *Geographic variation, speciation and clines*. Princeton Univ. Press, Princeton, NJ.
- Feng, S., J. Stiller, Y. Den, J. Armstrong, Q. Fang, A. H. Reeve, D. Xie, G. Chen, C. Guo, B. C. Faircloth, et al. 2020. et al. Dense sampling of bird diversity increases power of comparative genomics. *Nature* 587:252–257.
- Fernandes, A. M. 2013. Fine-scale endemism of Amazonian birds in a threatened landscape. *Biodivers. Conserv.* 22:2683–2694.
- Fernandes, A. M., J. Gonzalez, M. Wink, and A. Aleixo. 2013. Multilocus phylogeography of the Wedge-billed Woodcreeper *Glyphorhynchus spirurus* (Aves, Furnariidae) in lowland Amazonia: widespread cryptic diversity and paraphyly reveal a complex diversification pattern. *Mol. Phylogenet. Evol.* 66:270–282.
- Fernandes, A. M., M. Wink, C. H. Sardelli, and A. Aleixo. 2014. Multiple speciation across the Andes and throughout Amazonia: the case of the Spot-backed Antbird species complex (*Hylophylax naevius/Hylophylax naevioides*). *J. Biogeogr.* 41:1094–1104.
- Fitzpatrick, B. M. 2012. Estimating ancestry and heterozygosity of hybrids using molecular markers. *BMC Evol. Biol.* 12:1–14.
- . 2013a. HlEst: hybrid index estimation. R package version 2.0.
- . 2013b. Alternative forms for genomic clines. *Ecol. Evol.* 3:1951–1966.
- Frichot, E., F. Mathieu, T. Trouillon, G. Bouchard, and O. François. 2014. Fast and efficient estimation of individual ancestry coefficients. *Genetics* 196:973–983.
- Gay, L., P. A. Crochet, D. A. Bell, and T. Lenormand. 2008. Comparing clines on molecular and phenotypic traits in hybrid zones: a window on tension zone models. *Evolution* 62:2789–2806.
- Ghurye, J., M. Pop, S. Koren, D. Bickhart, and C. S. Chin. 2017. Scaffolding of long read assemblies using long range contact information. *BMC Genomics* 18:1–11.

- Gill, P. E., and W. Murray. 1974. Newton-type methods for unconstrained and linearly constrained optimization. *Math. Program.* 7:311–350.
- Glenn, T. C., N. J. Bayona-Vasquez, T. J. Kieran, T. W. Pierson, S. L. Hoffberg, P. A. Scott, K. E. Bentley, J. W. Finger, P. R. Watson, S. Louha, et al. 2017. Adapterama III: quadruple-indexed, triple-enzyme RADseq libraries for about \$1USD per Sample (3RAD). *bioRxiv* <https://doi.org/10.1101/205799>.
- Gompert, Z., and C. A. Buerkle. 2010. Introgress: a software package for mapping components of isolation in hybrids. *Mol. Ecol. Resour.* 10:378–384.
- . 2011. Bayesian estimation of genomic clines. *Mol. Ecol.* 20:2111–2127.
- . 2016. What, if anything, are hybrids: enduring truths and challenges associated with population structure and gene flow. *Evol. Appl.* 9:909–923.
- Gompert, Z., T. L. Parchman, and C. A. Buerkle. 2012. Genomics of isolation in hybrids. *Philos. Trans. R. Soc. B Biol. Sci.* 367:439–450.
- Gowen, F. C., J. M. Maley, C. Cicero, A. T. Peterson, B. C. Faircloth, T. C. Warr, and J. E. McCormack. 2014. Speciation in Western Scrub-Jays, Haldane's rule, and genetic clines in secondary contact. *BMC Evol. Biol.* 14:1–15.
- Greenwood, P. J. 1980. Mating systems, philopatry and dispersal in birds and mammals. *Anim. Behav.* 28:1140–1162.
- Gronau, I., M. J. Hubisz, B. Gulko, C. G. Danko, and A. Siepel. 2011. Bayesian inference of ancient human demography from individual genome sequences. *Nat. Genet.* 43:1031–1035.
- Gyllenstein, U., and A. C. Wilson. 1987. Interspecific mitochondrial DNA transfer and the colonization of Scandinavia by mice. *Genet. Res.* 49:25–29.
- Harrison, R. G. 1993. Hybrid zones and the evolutionary process. Oxford Univ. Press, Ithaca, NY.
- Hewitt, G. M. 1988. Hybrid Zones - natural laboratories for evolutionary studies. *Trends Ecol. Evol.* 3:158–167.
- Hill, G. E. 2019. Mitonuclear ecology. Oxford Univ. Press, Oxford, U.K.
- Johnson, E. I., and J. D. Wolfe. 2018. Molt in Neotropical birds: life history and aging criteria. 51st ed. American Ornithological Society CRC Press, Boca Raton, FL.
- Johnson, R., and D. W. Wichern. 1998. Applied multivariate statistical analysis. Prentice Hall, Englewood Cliffs, NJ.
- Jombart, T., and I. Ahmed. 2011. adegenet 1.3-1: new tools for the analysis of genome-wide SNP data. *Bioinformatics* 27:3070–3071.
- Kamm, J., J. Terhorst, R. Durbin, and Y. S. Song. 2020. Efficiently inferring the demographic history of many populations with allele count data. *J. Am. Stat. Assoc.* 115:1472–1487.
- Kawakami, T., R. K. Butlin, M. Adams, D. J. Paull, J. B. Steven, D. J. Paull, R. K. Butlin, and M. Adams. 2009. Genetic analysis of a chromosomal hybrid zone in the Australian Morabine grasshoppers (*Vandiemenna viatica* species group). *Evolution* 63:139–152.
- Leigh, J. W., and D. Bryant. 2015. PopART: full-feature software for haplotype network construction. *Methods Ecol. Evol.* 6:1110–1116.
- Li, H. 2013. Aligning sequence reads, clone sequences and assembly contigs with BWA-MEM. *arXiv:1303.3997v2*.
- Linck, E., and C. J. Battey. 2019. Minor allele frequency thresholds strongly affect population structure inference with genomic data sets. *Mol. Ecol. Resour.* 19:639–647.
- Liu, Y., J. Schröder, and B. Schmidt. 2013. Musket: a multistage k-mer spectrum-based error corrector for Illumina sequence data. *Bioinformatics* 29:308–315.
- Maia, R., H. Gruson, J. A. Endler, and T. E. White. 2019. pavo 2.0: new tools for the spectral and spatial analysis of colour in R. *Methods Ecol. Evol.* 10:1097–1107.
- McEntee, J. P., J. G. Burleigh, and S. Singhal. 2020. Dispersal predicts hybrid zone widths across animal diversity: implications for species borders under incomplete reproductive isolation. *Am. Nat.* 196:9–28.
- Mishmar, D., E. Ruiz-Pesini, P. Golik, V. Macaulay, A. G. Clark, S. Hosseini, M. Brandon, K. Easley, E. Chen, M. D. Brown, et al. 2003. Natural selection shaped regional mtDNA variation in humans. *Proc. Natl. Acad. Sci. USA* 100:171–176.
- Nadachowska-Brzyska, K., C. Li, L. Smeds, G. Zhang, and H. Ellegren. 2015. Temporal dynamics of avian populations during pleistocene revealed by whole-genome sequences. *Curr. Biol.* 25:1375–1380.
- Nei, M., and F. Tajima. 1981. Genetic drift and estimation of effective population size. *Genetics* 98:625–640.
- Nurk, S., A. Bankevich, D. Antipov, A. Gurevich, A. Korobeynikov, A. Lapidus, A. Prjibelsky, A. Pyshkin, A. Sirotkin, Y. Sirotkin, et al. 2013. Assembling genomes and mini-metagenomes from highly chimeric reads. Pp. 158–170 in M. Deng, R. Jiang, F. Sun, and X. Zhang, eds. *Research in computational molecular biology. RECOMB 2013. Lecture notes in computer science.* Vol. 7821. Springer, Berlin.
- Oswald, J. A., I. Overcast, W. M. Mauck, M. J. Andersen, and B. T. Smith. 2017. Isolation with asymmetric gene flow during the nonsynchronous divergence of dry forest birds. *Mol. Ecol.* 26:1386–1400.
- Phillips, B. L., S. J. E. Baird, and C. Moritz. 2004. When vicars meet: a narrow contact zone between morphologically cryptic phylogeographic lineages of the rainforest skink, *Carlia rubrigularis*. *Evolution* 58:1536–1548.
- Piálék, J., and N. H. Barton. 1997. The spread of an advantageous allele across a barrier: the effects of random drift and selection against heterozygotes. *Genetics* 145:493–504.
- Pulido-Santacruz, P., A. Aleixo, and J. T. Weir. 2018. Morphologically cryptic Amazonian bird species pairs exhibit strong postzygotic reproductive isolation. *Proc. R. Soc. Lond. Biol. Sci.* 285:20172081.
- Python Software Foundation. 2021. Python language reference. Python Software Foundation, Wilmington, DE.
- R Core Team. 2019. R: a language and environment for statistical computing. R Foundation for Statistical Computing, Vienna.
- Rambaut, A., M. A. Suchard, D. Xie, and A. J. Drummond. 2014. Tracer v1.6.
- Rhie, A., S. A. McCarthy, O. Fedrigo, J. Damas, G. Formenti, S. E. London, D. F. Clayton, C. V. Mello, and S. R. Friedrich. 2021. Towards complete and error-free genome assemblies of all vertebrate species. *Nature* 592:737–746.
- Ribas, C. C., A. Aleixo, C. Gubili, F. M. d'Horta, R. T. Brumfield, and J. Cracraft. 2018. Biogeography and diversification of *Rhegmatorhina* (Aves: Thamnophilidae): implications for the recent evolution of Amazonian landscapes. *J. Biogeogr.* 45:917–928.
- Rohland, N., and D. Reich. 2012. Cost-effective, high-throughput DNA sequencing libraries for multiplexed target capture. *Genome Res.* 22:939–946.
- Rohwer, S., E. Bermingham, and C. Wood. 2001. Plumage and mitochondrial DNA haplotype variation across a moving hybrid zone. *Evolution* 55:405–422.
- Sahlin, K., F. Vezzi, B. Nystedt, J. Lundeberg, and L. Arvestad. 2014. BESST - efficient scaffolding of large fragmented assemblies. *BMC Bioinformatics* 15:281.
- Schultz, E. D., J. Pérez-Emán, A. Aleixo, C. Y. Miyaki, R. T. Brumfield, J. Cracraft, and C. C. Ribas. 2019. Diversification history in the *Dendrocincla fuliginosa* complex (Aves: Dendrocolaptidae): insights from broad geographic sampling. *Mol. Phylogenet. Evol.* 140:106581.
- Semenov, G. A., E. Linck, E. D. Enbody, R. B. Harris, D. R. Khaydarov, P. Alström, L. Andersson, and S. A. Taylor. 2021. Asymmetric introgression reveals the genetic architecture of a plumage trait. *Nat. Commun.* 12:1–9.

- Shafer, A. B. A., C. R. Peart, S. Tusso, I. Maayan, A. Brelsford, C. W. Wheat, and J. B. W. Wolf. 2017. Bioinformatic processing of RAD-seq data dramatically impacts downstream population genetic inference. *Methods Ecol. Evol.* 8:907–917.
- Smith, B. T., M. G. Harvey, B. C. Faircloth, T. C. Glenn, and R. T. Brumfield. 2014. Target capture and massively parallel sequencing of ultraconserved elements for comparative studies at shallow evolutionary time scales. *Syst. Biol.* 63:83–95.
- Sorenson, M. D., J. C. Ast, D. E. Dimcheff, T. Yuri, and D. P. Mindell. 1999. Primers for PCR-based approach to mitochondrial genome sequencing in birds and other vertebrates. *Mol. Phylogenet. Evol.* 12:105–114.
- Stein, A. C., and J. A. C. Uy. 2006. Unidirectional Introgression of a sexually selected trait across an avian hybrid zone: a role for female choice? *Evolution* 60:1476.
- Szymura, J. M., and N. H. Barton. 1986. Genetic analysis of a hybrid zone between the Fire-Bellied Toads, *Bombina bombina* and *B. variegata*, near Cracow in southern Poland. *Evolution* 40:1141–1159.
- Thom, G., and A. Aleixo. 2015. Cryptic speciation in the white-shouldered antshrike (*Thamnophilus aethiops*, Aves - Thamnophilidae): the tale of a transcontinental radiation across rivers in lowland Amazonia and the northeastern Atlantic Forest. *Mol. Phylogenet. Evol.* 82:95–110.
- Thom, G., A. T. Xue, A. O. Sawakuchi, C. C. Ribas, M. J. Hickerson, A. Aleixo, and C. Miyaki. 2020. Quaternary climate changes as speciation drivers in the Amazon floodplains. *Sci. Adv.* 6:eaax4718.
- Toews, D. P., and A. Brelsford. 2012. The biogeography of mitochondrial and nuclear discordance in animals. *Mol. Ecol.* 21:3907–3930.
- Toews, D. P. L., A. Brelsford, and D. E. Irwin. 2014. Isotopic variation across the Audubon's-myrtle warbler hybrid zone. *J. Evol. Biol.* 27:1179–1191.
- Wang, M. S., M. Thakur, M. S. Peng, Y. Jiang, L. A. F. Frantz, M. Li, J. J. Zhang, S. Wang, J. Peters, N. O. Otecko, et al. 2020. 863 Genomes reveal the origin and domestication of chicken. *Cell Res.* 30:693–701.
- Wang, S., S. Rohwer, K. Delmore, and D. E. Irwin. 2019. Cross-decades stability of an avian hybrid zone. *J. Evol. Biol.* 32:1242–1251.
- Whitney, B. M., F. Schunck, M. A. Rêgo, and L. F. Silveira. 2013. A new species of flycatcher in the *Tolmomyias assimilis* radiation from the lower Sucunduri-Tapajós interfluvium in central Amazonian Brazil heralds a new chapter in Amazonian biogeography. Pp. 297–300 in J. del Hoyo, A. Elliott, J. Sargatal, and D. A. Christie, eds. *Handbook of the birds of the world*. Lynx Edicions, Barcelona, Spain.
- Wigginton, J. E., D. J. Cutler, and G. R. Abecasis. 2005. A note on exact tests of Hardy-Weinberg Equilibrium. *Am. J. Hum. Genet.* 76:887–893.
- Willis, E. O. 1969. On the behavior of five species of *Rhegmatorhina*, ant-following antbirds of the Amazon basin. *Wilson Bull.* 81:363–395.
- Wirtz, P. 1999. Mother species-father species: unidirectional hybridization in animals with female choice. *Anim. Behav.* 58:1–12.
- Woltmann, S., R. S. Terril, M. J. Miller, and M. L. Brady. 2010. Chestnut-backed Antbird (*Poliocrania exsul*) version 1.0. In T. S. Schulenberg, ed. *Birds of the world*. Cornell Lab of Ornithology, Ithaca, NY.

Associate Editor: B. Emerson
Handling Editor: A. G. McAdam

Supporting Information

Additional supporting information may be found online in the Supporting Information section at the end of the article.